Manuscript prepared for J. Name
with version 5.0 of the LaTeX class copernicus.cls.
Date: 24 April 2015

Feedbacks of dust via its impact on atmospheric stability during a dust storm in the Eastern Mediterranean

S. Rémy[1], A. Benedetti[2], A. Bozzo[3], T. Haiden[4], L. Jones[5], M. Razinger[6], J. Flemming[7], R.J. Engelen[8], V.H. Peuch[9], and J.N. Thepaut[10]

[1]Laboratoire de Météorologie Dynamique, Paris, France, European Centre for Medium-range Weather Forecasts, Reading, U.K.
[2-10]European Centre for Medium-range Weather Forecasts, Reading, U.K.

Correspondence to: S. Rémy
(samuel.remy@ecmwf.int)

Abstract.

Aerosols affect the atmosphere through the aerosol-radiation and the aerosol-clouds interactions. In this paper we report in detail on two feedbacks whereby the radiative effect of dust on surface radiative fluxes acts to decrease or increase the dust loading of the atmosphere via modification of boundary-layer stability, thereby acting to modify the radiative aerosol effect. These feedbacks between dust and boundary layer stability occurred during a series of dust storms in the Sahara and the Eastern Mediterranean in April 2012, which were studied using the Monitoring Atmospheric Composition and Climate - Interim Implementation (MACC-II) system.

The radiative fluxes in the short-wave and long-wave spectra were both significantly affected by the prognostic aerosols-radiation interaction, which in turn impacted the meteorological simulation. Reduced incoming solar radiation below the aerosol layers caused a decrease in maximum surface temperatures, and consequently a more stable thermal stratification of the lower atmosphere. The increased thermal stability led to decreased surface wind speeds and therefore to smaller amounts of dust emissions. On the other hand, horizontal gradients of surface temperature were increased at the edge of the dust plume, which led to local increases of surface wind speeds.

Larger downwelling long-wave fluxes were associated with the opposite processes: less stable thermal stratification at night, brought mainly by higher minimum temperatures at the surface, caused stronger surface winds. Regarding dust emissions, the impact by the short-wave radiative forcing was slightly more important than the long-wave contribution; this is in accordance with several previous studies. For surface temperature, short-wave and long-wave contribution appear to be close in intensity.

These feedbacks were amplified when taken into account in the aerosol analysis of the MACC-II global system. Taking them into account led to an improvement in forecasts of thermal radiative fluxes, minimum surface temperatures and dust Aerosol Optical Depth (AOD).

1 Introduction

1.1 Aerosol impacts on meteorology

Aerosol particles play an important role in the atmosphere through various mechanisms. They impact air quality and represent a serious public health issue, as shown by recent Particulate Matter (PM) pollution events in Western Europe and China (Zhang et al. (2013), Sun et al. (2013)). Aerosol particles also influence the atmospheric radiative budget through the aerosol-radiation interaction, also called aerosol direct effect(Yu et al. (2006),Bellouin et al. (2005)), by scattering and absorbing short-wave and long-wave radiation, and through the aerosol-clouds interaction or aerosol semi direct and indirect effect, by influencing the concentration, size and chemical composition of the cloud condensation nuclei (CCN), which in turn impacts the life cycle, the optical properties and the precipitation activity of clouds (Koch et al. (2010), Painemal et al. (2013), Hoose and Möhler (2012), Niemand et al. (2012)).

The aerosol direct effect consists of the sum of two phenomena: scattering/absorption of incoming solar radiation and absorption/emission of long-wave radiation. The former

reduces the amount of solar energy that reaches the surface and can cause a warming of the aerosol layer because of absorption. Aerosols also absorb and re-emit long-wave radiation, which increases down-welling long-wave radiation in and below the aerosol layer, and reduces night-time cooling of the surface. An aerosol layer thus acts on the radiative budget at the surface and in the lower atmosphere similar to a thin layer of clouds. The radiative impact of aerosols is very dependent on their vertical distribution: Choi and Chung (2014) showed that whether the aerosol layer is below or above a cloud layer will impact their radiative impact by an order of magnitude. Overall, on climatic time scales, the cooling impacts at the surface caused by the aerosol direct effect dominate over the warming effect: the radiative contribution of aerosols at the surface is estimated by the Intergovernmental Panel on Climate Change (IPCC) to be in the range of -0.3 W/m2 (Clouds and Aerosols. In: Climate Change 2013: The Physical Science Basis. Contribution of Working Group I to the Fifth Assessment Report of the IPCC (2013)). This is in line with the results of the AeroCom project (Schulz et al. (2006), Stier et al. (2013)), with a mean radiative impact of aerosols evaluated at -0.22 W/m2. In both cases, uncertainties on the radiative impacts of the aerosols are relatively high, associated with uncertainties on the quantification of aerosol sources and the interaction of aerosols with themselves and with the hydrological cycle interaction (Clouds and Aerosols. In: Climate Change 2013: The Physical Science Basis. Contribution of Working Group I to the Fifth Assessment Report of the IPCC (2013)).

As aerosol particles impact the radiative budget at the surface and also the thermal stratification of the lower atmosphere through the direct effect, other atmospheric processes are affected as well, in the Planetary Boundary Layer (PBL) and above. Increased surface temperatures at night will decrease the stability of the lower atmosphere, thus enhancing turbulent diffusion. Lower maximum temperatures will on the other hand decrease turbulent diffusion of heat. Since temperature and wind patterns are linked, the presence of an aerosol layer will also have an impact on wind patterns. Different heat diffusion and wind patterns can influence mesoscale and synoptic weather systems: Reale et al. (2011) for example showed that the African Easterly Jet (AEJ) was forecasted at an altitude and position that was closer to observations with interactive aerosols radiative effect. Heinold et al. (2008) also showed how the radiative effects of aerosols impacted the Low Level Jet (LLJ) in the Bodele depression of South Sahara, thus enhancing dust production. Dust aerosol events over the Eastern Atlantic could also impact hurricane activity over the Atlantic and Caribbean areas (Kamal et al. (2012) and S.H. Chen, personal communication, 2014).

Mineral dust are produced from arid or semi-arid areas and lifted into the atmosphere, if surface winds are strong enough, through the saltation process (Marticorena and Bergametti (1995)). Global emissions are estimated by numerical models to be in the range of 500 to 4400 Tg per year (Huneeus et al. (2011)). The large spread in emissions estimate reflect the fact that no observations of the dust emission amount are available. Out of the global amount, the Sahara desert contributes an estimated 400 to 2200 Tg per year. Major dust outbreaks frequently affect the Mediterranean, the Red Sea and the Atlantic : an estimated 20-30 Tg of dust is deposited each year in the Amazon Basin and contributes to the fertilization of the Amazon Basin (Yu et al. (2015)).

Most climate models now include aerosols and take into account their radiative impact on the atmosphere (Bellouin et al., 2011). For operational Numerical Weather Prediction (NWP) models, Tompkins et al. (2005) and Rodwell and Jung (2008) both showed that forecasts from European Centre for Medium-Range Weather Forecasts (ECMWF) operational model are improved when using an aerosol climatology to compute the aerosol radiative impacts. Mulcahy et al. (2014) investigated several configurations for the inclusion of interactive aerosol direct and indirect effects in the Met Office Unified Model (MetUM) and managed to correct a significant bias in the outgoing long-wave radiative fluxes over the Sahara that was diagnosed by Haywood et al. (2005).

Mineral dust and their impacts on climate have been the subject of intensive studies (eg Perez et al. (2006),Stanelle et al. (2010),Spyrou et al. (2013)), using numerical models developed by Tegen et al. (1996), Nickovic et al (2001) and Woodward (2001) amon others. Several results are summed up in Miller et al. (2014), which emphasizes the diversity of the results obtained in terms of radiative forcing by mineral dust.

This paper aims to document the interaction between the lower atmosphere and dust during a series of dust storm in the Sahara. In particular, the various feedbacks between the radiative impact of dust on the short-wave or long-wave spectra on one hand, and boundary layer meteorological processes on the other hand, were analyzed. The interaction of prognostic aerosols and meteorology were included at first only in the forward model, without any impact on the dust initial conditions. In a second step, they were included in the aerosol assimilation system so that the initial conditions of dust also took into account the impact of this interaction. Experiments using prognostic aerosols on one hand, and an aerosol climatology on the other hand for the computation of the aerosol-radiation interaction were compared. This allowed to assess the benefits of using prognostic aerosols instead of a climatology to estimate the aerosol impacts on meteorological fields.

1.2 The MACC global atmospheric composition forecasting system

The Monitoring Atmospheric Composition and Climate - Interim Implementation (MACC-II) is a European funded program that aims at monitoring and forecasting atmospheric composition. It is the precursor of the broader Copernicus Atmosphere Monitoring Service. MACC-II's aim is to create

and operate an assimilation and forecasting system for monitoring aerosols, greenhouse gases and reactive gases, using satellite observations and a combination of global and regional models (Hollingsworth et al. (2008), Peuch and Engelen (2012)).

Aerosols are forecasted within the MACC-II global system by a forward model (Morcrette et al. (2009), based on earlier work by Reddy et al. (2005) and Boucher et al. (2002)) that uses five species: dust, sea-salt, black carbon, organic carbon and sulphates. Dust aerosols are represented by three prognostic variables that correspond to three size bins, with bin limits of 0.03, 0.55, 0.9 and 20 μm. The main processes that are taken into account are production of dust through saltation and removal by dry deposition and sedimentation. The areas likely to produce dust are diagnosed as a function of surface albedo, moisture of the first soil level and bare soil fraction. Dust emissions are then parameterized, following Ginoux (2001), as a function of the cubic power of 10m wind speed. Dry deposition depends on a prescribed deposition velocity and on aerosol concentration in the lowermost model level above the surface. Sedimentation is currently applied only to the largest dust bin and depends on a fixed settling velocity and the concentration at each model level.

In the pre-operational version of the global MACC-II system, the radiative impact of aerosols is taken into account using the aerosol monthly climatology of Tegen et al. (1997). In an experimental version of the model, the aerosol direct effect can be computed from the prognostic aerosols provided by the MACC aerosol module. It is also possible to activate only the short-wave or the long-wave components of the aerosol direct effect separately. One of the objective of this study is to compare the results of this experimental version of the MACC-II system, which uses radiatively interactive aerosols, with the pre-operational setup, which uses an aerosol climatology to compute dust-radiation interaction. The radiative properties of aerosols were provided by E. Highwood from University of Reading; the experiments were also carried out with the radiative properties of aerosols used in the Hadley Centre climate model (Woodward (2001)) with similar results.

The global MACC-II forecasting system provides aerosol analysis by assimilating total Aerosol Optical Depth (AOD) observations provided by the Moderate Resolution Imaging Spectroradiometer (MODIS) instruments on-board NASA's polar orbiting satellites Aqua and Terra in a 4D-Var assimilation algorithm, as described in Benedetti et al. (2009). The product used in the assimilation step is the Dark Target retrieval, hence not available in regions with high surface albedo, such as desert areas. The use of the MODIS Deep Blue product, aimed at bright surfaces, is currently under investigation.

1.3 Evaluating aerosol impacts on Numerical Weather Prediction: WGNE model inter-comparison

The Working Group on Numerical Experimentation (WGNE) was jointly established by the Commission for Atmospheric Sciences of the World Meteorological Organization (WMO) and the World Climate Research Programme (WCRP). It has the responsibility of fostering the development of atmospheric circulation models for use in weather, climate, water and environmental prediction on all time scales and diagnosing and resolving shortcomings of these models. WGNE has recently launched a model inter-comparison aimed at improving the understanding of aerosol impacts on numerical weather prediction. Three case studies were proposed to the participants: a severe anthropogenic pollution case in January 2013 in Northern China, a biomass-burning event in Brazil in September 2012 and a dust storm over Egypt on 18th of April 2012. This paper focuses on the dust episode of 18th of April 2012 over the Eastern Mediterranean. Another dust storm, which took place on 12th and 13th of April 2012 in the Central Sahara region was also studied, as more ground observations were available.

2 Dust episodes of April 2012 in the Sahara and Eastern Mediterranean

2.1 Available observations

Surface observations of meteorological parameters in Algeria and Egypt were used to analyze the meteorological situation. Observations were not available over Libya because of the political situation in this period. Daily weather charts from the Berlin University and the UK Met Office were also used to assess the synoptic evolution of the dust storm.

Observations are much sparser for radiative fluxes than for meteorological parameters. The Baseline Surface Radiation Network (BSRN) (Heimo et al. (1993))maintains two stations in the area of interest: Tamanrasset (Mimouni (2013)) in Southern Algeria and Sede Boqer in Israel (Lyubansky (2012)). Unfortunately, observations from Sede Boqer were not available in April 2012. Downwelling surface flux of short-wave and long-wave radiation at Tamanrasset, in Southern Algeria, were measured with a frequency of 1 minute. A climatology of daily downward surface solar flux has been established by Satellite Application Facility on Climate Monitoring (CM-SAF, Stengel et al. (2013)), derived from remote sensing by the Spinning Enhanced Visible and Infrared Imager (SEVIRI) sensor onboard MeteoSat Second Generation (MSG), with an accuracy of 20 W/m2.

Finally AOD observations were available from the AErosol RObotics NETwork (AERONET, Holben et al. (1998)) of ground observations. The stations used in this study are Tamanrasset, collocated with radiative fluxes ob-

servation from BSRN, and Cairo in Egypt. As these observations are provided by sun photometers, they are available only during the day. To supplement the absence of AOD observations at some stations, simulated AOD was also plotted to provide a qualitative assessment of the presence of dust. Total AOD observations are also available from MODIS over desert areas, using the Deep Blue algorithm (Shi et al. (2013)).

2.2 Sahara dust storms of April 2012: synoptic evolution

Dust storms are a frequent occurrence in the Sahara, where dust production areas are widespread. As the soil is generally very dry in these regions and predominantly composed of sand, surface temperatures can reach very high values in April. Higher altitude colder air from Mediterranean lows occasionally affects the area. The severe dust storm that affected Libya, Egypt and most of the Eastern Mediterranean basin on 17th-18th of April 2012 was produced by the conjunction of a deep low circulating over the Mediterranean and of a heat low that originated over Western Libya-Eastern Tunisia on 16th of April 2012, caused by very high temperatures over the desert areas. Figure 1 shows mean sea-level pressure analyses over Northern Sahara and Southern Mediterranean from 17th to 19th of April 2012. The merging and interaction of the heat low and the Mediterranean low that is associated with mid-tropospheric colder air is clearly shown. This interaction, and the development of a powerful anticyclone over the central Sahara, led to the rapid deepening of a low between Crete and Greece on 18th of April. The heat low moved in a North-Easterly direction, left Western Egypt in the night of 17th to 18th of April, and was then absorbed by the larger and fast moving Mediterranean low, which then moved quickly towards the North on 19th of April 2012.

The synoptic situation led to high and sustained winds on 17-18 of April over North East Libya and Egypt associated with a cold front crossing these regions, reaching 11 to 14 m/s for more than 24 hours, according to model forecasts and observations. This led to the suspension of a very high load of dust, with AOD reaching 4.5 in Cairo at noon on 18th of April. Besides the dust plume, the sky was entirely clear over Egypt and Libya during 17th and 18th of April, which makes these two days a perfect case study for aerosol-radiation interaction.

The interaction between dust and the synoptic situation is shown by Figure 2, which shows daily AOD over Eastern Sahara from the Deep Blue algorithm applied to MODIS/Aqua observations. The large dust load that was lifted by cold front associated with the heat low was then advected Northwards by the deep Mediterranean low, towards Israel, Turkey and the Eastern Mediterranean on 18-19 April 2012.

Figure 3 shows the evolution of the dust storm as analysed and forecasted by the MACC system, from 17 April 2012 6UTC to 18 April 2012 12UTC. Dust AOD reaches very high values, locally above 4. The area with AOD above 1 is very large throughout the storm.

This dust storm was preceded by another event between 11th and 15th of April 2012, that affected the central Sahara up to Libya and Western Egypt. This was caused by a persistent and slow moving heat low over central Sahara combined with a deep low over Western-central Mediterranean. This event was also studied as the whole of April 2012 was forecasted by the global MACC-II system in the framework of the WGNE model inter-comparison. This allowed comparing forecasts of radiative fluxes against ground observations at Tamanrasset (Algeria), which was affected by the dust storm of 11th to 15th of April but not by the following storm of 17-18 April 2012.

3 Methodology

The objective of this study is to assess the impact of the aerosol direct effect on the forecasted meteorological parameters during the dust storms that affected the Sahara and Eastern Mediterranean basin in April 2012. To achieve that, the MACC-II global system was run with the aerosol direct effect estimated from a climatology, i.e. in its pre-operational configuration, or from prognostic aerosols. All runs were carried out with a T_L511 horizontal spectral resolution which corresponds to a grid-box size of about 40km. 60 vertical hybrid sigma-pressure levels were used, the lowest level being 17m above the surface.

3.1 Cycling forecasts

In this configuration, the model is run without assimilating AOD. The meteorological fields are initialised from the global MACC-II analysis, and the aerosol fields were initialised from the MACC re-analysis on the 10th of April 2012 only and otherwise from the previous 24h forecast. In this configuration the aerosol fields are not constrained by any observations and could drift away from observed values.

The main advantage of this configuration comes from comparing the model outputs with and without radiatively interactive aerosols. Since the meteorological analyses are the same for all the experiments, the differences between the meteorological forecasts originate only from the way interaction between aerosols and radiation are computed, i.e. using prognostic aerosols or a climatology. Cycling forecasts are thus adequate to assess the aerosols' impact on forecasted meteorological fields.

A default for this configuration is that since the meteorological analysis are provided by another simulation, in this case by the MACC-II Near Real Time (NRT) system, the interaction between aerosols and meteorology is reset at every forecasting cycle. Experiments were carried out with both aerosols and meteorological fields initialised from the

previous 24h forecast, and they showed the same results qualitatively than when meteorological fields were initialised from the global MACC-II analysis. The amplitude of the aerosol-meteorology interaction was however significantly larger since it was also included in the meteorological analysis.

Cycling forecasts were carried out for the period from 10th to 30th of April 2012, every 24h, with runs starting at 00UTC. July 2012 was also run, in order to check if the conclusions reached for April 2012 are also valid globally for other periods of time.

3.2 Short-wave and long-wave aerosol direct impact

Since the physical phenomena that underlie the aerosol direct effect are not the same in the short-wave and in the long-wave spectra, these two contributions can be separated in the MACC-II global system. It is now possible to compute the total radiative impacts of aerosols, using prognostic aerosols in the short-wave spectrum and the aerosol climatology of Tegen et al. (1997) in the long-wave spectrum, and vice-versa. As a consequence, it is possible now to decompose the prognostic aerosol direct effect (or "Total aerosol effect") in its "Short-wave aerosol direct effect" and "long-wave aerosol direct effect" components.

The following experiments were carried out with cycling forecasts:

- NOAER : experiment with no dust aerosols,
- REF: Reference experiment with the aerosol direct effect computed from an aerosol climatology,
- LW: The long-wave component of the aerosol direct effect is computed using prognostic aerosols, the short-wave part is computed with an aerosol climatology,
- SW: The short-wave component of the aerosol direct effect is computed using prognostic aerosols, the long-wave part is computed with an aerosol climatology,
- TOTAL: Both the short-wave and the long-wave components of the aerosol direct effect are computed using prognostic aerosols

Our reference run uses aerosol direct effect computed from an aerosol climatology, as this corresponds to the current pre-operational configuration of the system. This allows us to compare the current configuration of the model with the envisaged evolution towards using interactive aerosols to compute dust-radiation interaction. Figure 4 shows the time evolution at Tamanrasset of observed and forecasted downward radiative fluxes and 2m temperature for the NOAER and REF experiments. As the Tegen aerosol climatology that is used in the REF experiments provide rather small values of dust AOD for this period, close to 0.3, the impact on radiative fluxes is also rather small: in the order of 1W/m^2 for long-wave fluxes and 20-30 W/m^2 for short-wave fluxes. Maximal and minimal temperatures are slightly effected by this changes in radiative fluxes, by around 0.1 to 0.2K.

3.3 Assimilation runs

In this configuration the model is run with the full 4DVar data assimilation, providing initial conditions for both the aerosol and meteorological variables. The following experiments were carried out with assimilation runs:

- REF_ASSIM: Reference experiment with the aerosol direct effect computed from an aerosol climatology,
- TOTAL_ASSIM: the aerosol direct effect is computed using prognostic aerosols.

Runs were carried out at 0 and 12 UTC every day for the whole of April 2012, with an assimilation window of 12 hours. However, only the runs of 00UTC go beyond 12 hours of forecast time. As a follow-up to cycling forecasts, assimilation runs will allow to study how using radiatively interacting aerosols in the forward model affect initial conditions through the data assimilation.

Table 1 provides a summary and a short description of the experiments carried out.

4 Impact of the dust on radiative fluxes

In this section, forecasts of the REF and TOTAL experiments are evaluated against ground observations of radiative parameters. Figure 5 shows a time-series of observed and modelled surface downward long-wave and short-wave radiative fluxes at the surface, top of atmosphere (TOA) and AOD at Tamanrasset and Cairo. Tamanrasset was mostly affected by the dust storm from 12th to 14th of April; high clouds were also present at times from 10th to 13th of April whereas Cairo was impacted by high dust load mainly on 15 and 18 April.

It is hard to separate the effect from the radiative impact of clouds and of aerosols during 10-13 April at Tamanrasset. Observations show that during this period, when clouds and aerosols are present, the diffuse component of incoming solar radiation is increased (not shown) whereas direct solar radiation is nearly halved: maximal total solar radiation is 200 to 300 W/m2 smaller on 12 and 13 April compared to 14-18 April. Observed downward long-wave fluxes at the surface are on average around 60 W/m2 higher on these two days. As the observed clouds are mainly high clouds, which have little effect on the downward long-wave flux at the surface, it is likely that this difference in the observations is caused mainly by the presence of dust particles on 12-13 April.

LW downward radiation is increased by 10-20 W/m^2 on 12-13 April at Tamanrasset, and by 20-30 W/m^2 on 15 and 18 April at Cairo, showing that the aerosol burden provided by the aerosol scheme is larger than what is given by the Tegen

climatology. This increase helps reduce a negative bias of close to 20 W/m^2 in the forecasted LW fluxes at Tamanrasset. The downward solar surface flux (DSSF) is decreased by 50 to 100 W/m^2 on 12-13 April at Tamanrasset, and by more than 250 W/m^2 on 18 April at Cairo, reflecting the scattering effect of the aerosol layer. On 14, 16 and 17 April, at Tamnrasset, the predicted dust AOD is very low, lower than the values provided by the Tegen climatology : this is reflected in the slightly higher forecasted DSSF by TOTAL on these days.

At TOA, outgoing long-wave radiation (OLR), is smaller for TOTAL by 5-10 W/m^2 on 12-13 April at Tamanrasset and by up to 20 W/m^2 at Cairo. The negative sign corresponds to a convention at ECMWF whereby fluxes from surface are negative and fluxes towards the surface are positive. The order of magnitude in OLR difference between REF and TOTAL is in agreement with the results of Haywood et al. (2005) and Mulcahy et al. (2014). The difference is most important during day-time because, in the absence of clouds, OLR is driven mainly by surface temperature, which is lower for TOTAL as compared to REF during day-time. The overall effect is rather small : on average, the OLR at TOA is only 2-3W/m^2 smaller for TOTAL. SW radiation is also smaller at TOA for TOTAL because of increased columnar absorption over the bright desert surface. The difference reaches 30-50 W/m^2 at Tamanrasset on 12-13 April and more than 100 W/m^2 at Cairo on 18 April. On average, SW radiation at TOA is 14-16 W/m^2 lower for TOTAL.

5 Impact of the dust-short-wave radiation interaction on boundary layer meteorological processes

In this section, the impact of the solar aerosol-radiation interaction on meteorological parameters and dust production is investigated. Figure 6 shows observed (when available) and forecasted meteorological parameters, dust production flux and 550nm AOD at Cairo and at the Siwa Oasis, which lies at 29 °12'N, 25 °29'E, for the REF and the SW experiments. The latter location was chosen because it was affected by the dust storm from the morning of 17 April to the afternoon of 18 April whereas Cairo was mainly affected around midday on 18 April. Sensible heat flux is negative during the day because of a sign convention at ECMWF : a negative value indicates that the surface heats to the atmosphere, a positive one, that the surface cools it.

The strong radiative forcing in the short-wave (cf figure 5) influences maximum temperatures : they are 3 degrees lower for the SW experiment on 18 April at Cairo, and 2-3 degree lower on 17 April at Siwa. On average, this increases a small negative bias, from -0.1K for REF to -0.4K for SW at Cairo, and from -0.8K to -1 K a Siwa. As the surface is less hot during the day with SW, the sensible heat flux also decreases by up to 150 W/m^2 on 18 April 2012 at Cairo. The impact is small at Siwa, since the impact of lower solar ration on 2m temperature, representative of surface heating, was mainly felt after the solar maximum of 17 April and before the solar maximum of 18 April. The sensible heat flux is lower by around 50 W/m^2 on 17 April.

Associated with lower maximal temperature and sensible heat flux at midday is a decrease of wind speed at 10m. Wind speed during day-time is 1 to 1.5 m/s smaller with the SW experiment on 17 April at Siwa and on 18 April at Cairo. This can be explained by the fact that with lower maximum temperatures the planetary boundary layer (PBL) is less unstable; as a consequence the wind profile associated with the thermal stratification tends to be more logarithmic and surface winds tend to be weaker. For surface winds, bias and root mean square error (RMSE) are very close between SW and REF.

Not unexpectedly, dust production is smaller with SW because of lower wind speed at surface. The dust production flux is nearly 25% lower with REF at midday on 18 April at Cairo, and 15-25% lower in the second half of 17 April and also at midday on 14 April at Siwa. Since dust production is around 30 times larger at Siwa than at Cairo during the storm, because of stronger winds, the absolute impact on dust production is much larger for Siwa : the difference between REF and SW is around 20 times larger at Siwa than at Cairo. The fact that dust production is more active at Siwa than at Cairo shows that the dust layer is mainly advected at Cairo, whereas it is both advected and produced at Siwa.

As a consequence of smaller emissions, AOD itself is overall slightly lower for SW. The impact is rather small at Cairo, where the dust storm is mainly advected from the West : dust AOD is on average 0.03 lower for SW, the difference reaching 0.2-0.3 on the morning of 18 April. At Siwa, where dust production contributes significantly to the dust layer, AOD is lower by 0.05 on average, and by more than 0.5 on the afternoon and evening of 17 April. A bit further to the North-West, closer to the heart of the dust storm, the AOD difference reaches nearly 1.

To better understand the interaction between dust and meteorology, Figure 7 shows the difference between SW and REF for a set of meteorological parameter, for a 36h forecast starting on 17 April 2012 0UTC. This is close to the local solar maximum in Egypt and Libya. The region where 2m temperature is lower for SW matches nicely the region where dust AOD is high, as shown on Figure 3. Temperature at 850 hPa is also generally lower for SW as compared to REF, but by a smaller margin as compared to 2m temperature. While for 2m temperature the difference between the two experiments is 1-3K in the regions with AOD above 1, at 850 hPa, the difference is between 0.5 to 1.5K. This differential impact of surface and 850 hPa temperature affects the thermal stratification of the PBL and is one cause for generally lower wind speed at 10m and dust production. A band of higher surface wind speed and dust production lies at the W of Lake Nasser, showing that the modification of the thermal

stratification of the atmosphere is not the only phenomenon that impacts winds and dust production.

Stronger or weaker winds can be caused by a combination of the following factors:

- Synoptic causes: the pressure gradient and geostrophic component of winds could be larger or smaller,
- Dynamic thermal causes: the horizontal temperature gradient impacts the wind speed,
- Local causes: a different thermal stratification of the boundary layer modifies the vertical structure of the winds in the boundary layer.

Figure 7 also shows the difference between SW and REF for mean sea-level pressure and wind speeds at 925 hPa. Wind speeds at 925 hPa are less influenced by surface properties and should be more representative of the large-scale component of wind speed. They are less impacted by SW as compared to surface wind speeds, which shows that synoptic factors are less important than the local factors to explain the lower wind speeds of SW. Surface pressure is everywhere higher with SW by 0.5 to 1 hPa in general. As this increase is rather low, and since its repartition is quite uniform (it is well collocated with the area where 2m temperature is significantly lower with SW), geostrophic wind is not much changed between SW and REF : synoptic factors are not the predominant cause of the wind speed and dust production decrease under the dust layer.

However, thermal stratification doesn't account for the higher wind speed and dust production at the Eastern edge of the dust storm, W of Lake Nasser. Figure 8 shows that the area where surface wind speed is higher for SW corresponds to an area of important horizontal thermal gradient associated with the cold front that is causing the dust storm. From E to W, 2m temperature decreases by more than 10K in no more than a few hundred kilometers along the 22N parallel. The western part of this high gradient area is heavily impacted by the reduced incoming solar radiation : 2m temperature there is up to 2K smaller with SW. The eastern part is in front of the dust storm and not yet affected by it : the dust load is not very high there and temperatures are reduced by 0.5 to 1K. The differential impact of the dust layer on 2m temperature thus increases the horizontal gradient in this region by more than 1K.

This is clearly shown by figure 9, which presents a cross-section of surface pressure, temperature and wind speed along the 22N parallel. The pressure gradient is slightly larger for SW than for REF : 1.2 hPa against 1 hPa. The horizontal thermal gradient is 5K from 29 to 30E for REF, more than 6K for SW. Thermal wind is directly impacted by the horizontal gradient of temperature through the thermal wind equation (Holton (2004)) :

$$\mathbf{v}_T = \frac{R}{f} \ln \left[\frac{p_0}{p_1} \right] \mathbf{k} \times \nabla_p \bar{T} \quad (1)$$

Where R is the specific gas constant for air, f is the Coriolis parameter, k is the vertical unit vector and the subscript p on the gradient operator denotes a gradient on a constant pressure surface. In this case, the increase in the horizontal gradient of surface temperature is the predominant factor of an increase of surface wind by around 2m/s at 22N 29.5E.

To sum up, the aerosol-radiation interaction in the shortwave is at the origin of two feedbacks between aerosol and meteorology : a negative one that is driven by the differential changes between temperature at surface and at the top of the PBL, which in turn increases thermal stability of the PBL, decreases surface winds and dust production. A local positive feedback can occur at the edge of the dust layer, where during day-time the horizontal temperature gradient is locally increased by the differential impact of the dust layer on surface temperatures. This increase in horizontal gradient increases in turn wind speed and thus dust production. As Figure 10 shows, the overall difference SW-REF for dust AOD is negative, which means that the negative feedback, driven by local factors, is predominant compared to the local positive feedback driven by dynamical factors.

6 Impact of the dust-long-wave radiation interaction on boundary layer meteorological processes

In this section, the impact of the thermal aerosol-radiation interaction on meteorological parameters and dust production is investigated. Figure 11 shows observed (when available) and forecasted meteorological parameters, dust production flux and 550nm AOD at Cairo and at the Siwa Oasis for the REF and the LW experiments.

2m temperature is higher during the nights for the LW experiment, since the dust aerosol layer emits downwards in the long-wave (cf Figure 5). The overall impact is rather small, 0.3K at Cairo and 0.4K at Siwa, but on the nights concerned with high dust load, the difference can reach up to 1.5K for Cairo the nights of 17-18 and 18-19 April, and up to 2K for Siwa the night of 17-18 April, which helps to reduce a cold bias. At Cairo, the day-time temperatures are also significantly higher with LW, by 0.5 to 1K. This translatesinto slightly larger sensible heat fluxes, by close to 30 W/m^2 at midday on 18 April at Cairo. At Siwa, night-time cooling is significantly reduced, and even partially reversed, on the night of 17-18 April. At the beginning of the night, the sensible heat flux is slightly positive for REF, which indicates a cooling of the surface, and slightly negative for LW.

Clear-sky nights are generally characterized by very stable PBLs over the desert since the heat capacity of sand is small compared to other soil types. This very stable PBL is in turn at the origin of the nocturnal low level jet (NLLJ). NLLJs in North Africa can be formed by different mechanisms; here the driving mechanism is an inertial oscillation (Knippertz (2008), Van de Wiel et al. (2010)), which compensates the low value of surface winds caused by surface friction and

very high PBL stability by a low-level jet that lies under the top of the PBL, with wind values above the geostrophic wind values. NLLJs are an important driver for dust emission in North Africa (Fiedler et al. (2013),Heinold et al. (2013),Heinold et al. (2014)). Higher nocturnal surface temperatures under the layer of dust with LW decrease the PBL stability, thus locally increasing surface wind speeds. This interaction between aerosol and meteorology might weaken the NLLJs over this area.

The impact on surface wind speed is very small at both Cairo and Siwa. As dust production is a cubic function of surface wind speed, the impact of the small increase of the surface wind speed is significant on dust production. It is larger with LW by up to 15% at midday on 18 April at Cairo, and by up to 20% in the evening of 17 April at Siwa. This affects only marginally AOD at Cairo, however the difference is not negligible at Siwa, where AOD maximum during the night of 17-18 April is increased by nearly 0.5. Figure 10 shows that on the night of 17-18 April, the area where AOD is larger by more than 0.3 with LW is important and is well collocated with the area of high dust load (cf Figure 3).

Figure 12 shows the difference on 18 April 0UTC between LW and REF for a set of meteorological parameters as well as dust production. 2m temperature is larger for LW on most continental surfaces, by 0.3 to 0.5K in regions where the dust load is not very important, and by 1 to 2.5K in regions where dust AOD exceeds 2. This difference is caused by emission in thermal spectrum by the dust layer. Most this layer lies below 850 hPa in the nocturnal PBL. Temperatures at 850 hPa are affected in a different measure as surface temperature and over most areas they are slightly lower for LW. Over a band that corresponds to the cold front, 850 hPa temperature is higher by 0.2-0.5K. This different impact of longwave aerosol-radiation interaction between surface and 850 hPa affects strongly the stability of the PBL.

A less stable boundary layer with LW is associated with slightly stronger winds at surface, by 0.3-1 m/s over most areas. The area of higher 850 hPa temperatures with LW is associated with weaker surface winds, by 0.5 to 1 m/s. At 925 hPa, the pattern of wind change is more complex, with a marked dipole pattern, which suggest that the cold front characteristics are modified by the LW experiment. Higher temperatures at surface are associated with lower surface pressure, by 0.5 to 1hPa. As the decrease in pressure decrease occurs behind the cold front, in a region where pressure is building up after the front, this process decreases slightly the pressure gradient and thus geostrophic wind behind the cold front.

The predominant increase in surface winds translates into mostly larger dust emissions. The notable exception is the area with lower surface wind speeds that lies just before the cold front. As a consequence, dust AOD is generally larger for LW (see Figure 10); however, values are significantly lower just before the cold front.

To understand better the phenomena taking place around the cold front, Figure 13 presents a cross-section of various meteorological parameters along the 22N parallel. The pressure gradient along 22N is only marginally modified by LW. However, 2m temperature is more than 1.2K higher with LW at 22E, and only 0.6K higher at 22.5E. This increases the horizontal temperature gradient and thus thermal wind directed towards the West. As the synoptic wind associated with the cold front blows from the West, this increase in thermal wind actually provokes an important decrease in 10m wind speed. This is especially apparent in the longitudinal component of 10m wind, which contributes to a large part of the decrease in surface wind between 22.5E and 23E. The same horizontal thermal gradient factor can explain the increase of surface winds for LW between 23E and 23.5E. The pressure gradient between 23E and 23.5E is nearly flat for LW, significantly lower than for REF; as a consequence, geostrophic winds are also lower. The fact that surface winds are stronger there for LW can also weaken the NLLJ mechanism, which would contribute to a lower wind speed at 925 hPa.

The mechanism whereby thermal winds are increased, and surface wind speed decreased, by a differentiated aerosol-radiation interaction in the long-wave is actually a self-enhancing one, i.e. a positive feedback. Lower dust AOD in front of the dust storm means a less intense night-time warming by thermal radiation by the dust layer. This in turn increases Westward thermal wind, as the temperature gradient increases more with LW under the cold front than just before. This in turn decreases surface wind speed, as the increased thermal component of the wind goes against synoptic winds from the West associated with the cold front. This reduces dust emissions and in turn dust AOD. This positive feedback is apparent in figure 10 : the area before the cold front with lower dust AOD is larger and more intense after 36h of forecast as compared to 24h forecast.

To sum up, the aerosol-radiation interaction in the long-wave is at the origin of two feedbacks between aerosol and meteorology : a positive one that is driven by the differential changes between temperature at surface and at the top of the PBL, which in turn decreases thermal stability of the PBL, increases surface winds and dust production. A local negative feedback can occur at the edge of the dust layer, where during night-time the horizontal temperature gradient is locally increased by the differential impact of the dust layer on surface temperatures. This increase in horizontal gradient increases in turn thermal wind towards the cold front, which decreases surface winds as it blows mainly from the cold front. Dust production and AOD are likewise affected, thus enhancing this negative feedback.

7 Interaction of total aerosol radiative impact

In this section, the reference experiment is compared against TOTAL, which uses prognostic aerosols to compute aerosol-

radiation interaction in both SW and LW spectra. Figure 14 shows 3-24h forecasts of a set of meteorological parameters together with dust production and AOD at 550nm for REF and TOTAL, at Cairo and Siwa Oasis.

At Cairo, which was affected by the dust storm mainly during day-time on 18 April, sensible heat flux and 10m wind speed are very close between the SW and TOTAL experiments. For 2m temperature however, the impact of the short-wave and of the long-wave is equally felt : maximum temperature on 18 April is significantly lower than REF with both SW and TOTAL, but more so with SW (3K difference) than with TOTAL (2K). The thermal emissions of the dust layer also play a role, with slightly higher minimal temperatures on the mornings of 15, 18 and 19 April. On average, the bias on 2m temperature is unchanged for TOTAL as compared to REF, against an increase of the cold bias from -0.1K to -0.4K for SW, and a warm bias of 0.2K for LW. While bias is unchanged with TOTAL, RMSE is slightly decreased as compared to REF.

As the dust production maximum occurs at midday on 18 April at Cairo, the impact of SW aerosol-radiation interaction is predominant; however, the LW aerosol-radiation influence is not negligible as dust production is around 10% larger to TOTAL as compared to SW. At the height of the dust storm, dust production is reduced by around 10-15% for TOTAL against 25% for SW as compared to REF. Similarly, dust AOD is reduced with TOTAL as compared to REF, but by a much smaller amount as compared to the reduction with SW.

At Siwa, the dust storm lingered on longer than at Cairo, was more intense, and was most intense during the night. Depending on the weather parameters and of the time scales of the meteorological processing affecting them, the influence of the SW or of the LW aerosol-radiation interaction was predominant. For 2m temperature, the impact of SW was noticeable on the maxima on 17 April. The LW impact was felt mainly on the nights of 15 and 18 April, and on average temperature was marginally higher for TOTAL as compared to REF, but by a smaller amount as compared to LW. Sensible heat fluxes were also larger for TOTAL, but the decrease in sensible heat caused by reduced incoming solar radiation on 17 April caused this increase to be smaller than for LW. 10m wind speed was not much affected by both LW and SW, this is is the same for TOTAL, with values marginally smaller than for REF on average, but slightly larger on the early morning of 18 April. Likewise, dust emissions are significantly smaller for TOTAL on 14 April, with a dust lifting episode occurring nearly entirely during day-time, and is at times smaller at times larger for the dust storm of 17-18 April. Dust emissions are smaller by around 10% with TOTAL during day-time of 17 April, and 5-10% larger in the early morning of 18 April. Dust AOD at 550nm reflects the influences of both dust-SW and LW radiation. In the evening of 17 April, after several hours with smaller dust emissions with TOTAL, dust AOD is lower by around 0.4, i.e. 12% of the total. Dust AOD then increases faster with TOTAL than with REF, and values are very similar for both experiments on 18 April.

Figure 15 shows the difference between TOTAL and REF for 2m temperature, 10m wind speed, dust emissions and dust AOD at 550nm, at 0UTC and 12 UTC on 18 April for a simulation starting on 17 April at 0UTC. These hours were chosen as they are close to the peak of impact of dust-LW and SW interaction respectively, Figure 15 can be compared with Figure 12 and Figure 7. The radiative impact in the SW and LW are evident in the 2m temperature difference plots: the areas where temperature is more than 1K higher with TOTAL at 3UTC and where temperature is more than 1K lower with TOTAL at 12UTC are in the same range. Compared to the values of SW and LW experiments on Figures 7 and 12, the differences are smaller. This is expected, as higher minimal temperatures mitigate the impact of weaker solar heating during the day, and vice-versa.

The impact on wind speed is similarly of the same nature as SW and LW for day and night respectively, but reduced in amplitude. As for SW and LW, a positive (resp. negative) feedback develops at the edge of the dust plume, just before the cold front. As these feedback are symmetrical between SW and LW, they are destroyed when the driving forcing, i.e. reduced solar heating and thermal emission by the dust layer respectively, is replaced by the alternative forcing. This is why the areas where thermal winds change affect winds and dust emission are the same between SW during the day, LW during the night on one hand, and TOTAL and the other hand, but much reduced in intensity. As these structures are transitory, they have less impact on dust emissions and dust AOD than in the SW and LW experiments. The areas where winds are decreased (by 0.2-0.8 m/s) or increased (by 0.5-1 m/s) by the changes in thermal stratification of the PBL are on the other hand clearly visible; dust emissions reflect the changes in wind speed. The impact of these two conflicting changes appear to be of similar amplitude, as total AOD changes are much smaller for TOTAL as compared to SW or LW.

Figure 16 presents vertical profiles of dust mixing ratio, temperature and wind speed over the Siwa Oasis, at 15UTC on 17 April and 12 UTC on 18 April, for a simulation starting on 17 April 0UTC and for REF and TOTAL. The cold front passed in between the two forecast times, which is clearly shown in 850 hPa temperatures, which are more than 10K colder at 3UTC than at 15UTC on 17 April.

The mixing ratio profiles show that dust is mainly confined in the boundary layer, the top of which is at around 800 hPa at 15 UTC and just above 950 hPa at 3UTC. The impact of the meteorology on dust emissions, already noted, is again clear here : dust mixing ratio is 20 to 50% lower with TOTAL at 15 UTC, and is slightly larger at 3UTC. The impact on temperatures is clear : light scattering occurs in the dust layer and reduces temperatures by 1-2K below 925 hPa at 15 UTC for TOTAL, and by a smaller amount, less than O.5K,

between 800 and 925 hPa. At 3UTC, thermal radiation from the dust layer provoke a small increase in temperature for TOTAL very close to the surface, below 970 hPa. Above that height, temperature is slightly lower for TOTAL, because the dust layer absorbs a part of the radiation from the surface. Winds for TOTAl are slightly weaker at 15 UTC at surface, and slightly stronger at 3 UTC. Above the surface, winds are mostly stronger at 15 UTC, by up to nearly 1m/s at 750 hPa. At 925 hPa with TOTAL, there is a small temperature inversion, as the aerosol layer cools the atmosphere below that height. Associated with this small temperature inversion is a significant increase of wind speed, by around 1m/s. At 3 UTC, winds are stronger just above the top of the PBL, by around 1m/s.

To sum up, TOTAL is a composition of LW and SW: the mainly positive feedback between dust and meteorology associated with LW and the mainly negative feedback associated with SW co-exist and also impact each other. The local feedbacks before the cold front, driven by horizontal thermal gradients, neutralize each other and are thus much smaller in amplitude in TOTAL as compared to SW and LW. This shows that the timing of the storm, and whether it is primarily affected by the dust-SW or LW radiation interaction are of great importance to understand how the dust layer impacts meteorology and vice-versa. In this case, it appears that the dust-radiation interaction didn't impact much the synoptic situation, i.e. the motion of the highs and lows as well as the movement and intensity of the cold front that caused the storm. Cycling experiments, with a meteorological analysis that is provided by the NRT MACC-II system, are not the best tool however to assess the synoptic impact of dust-radiation interaction. Assimilation runs provide a better insight into this issue.

8 Assimilation runs

Figure 17 shows the differences between the experiments TOTAL_ASSIM and REF_ASSIM for 2m temperature, 10m wind speed, dust production and dust AOD at 550nm for the runs starting at 00UTC on 17 April 2012, 24 and 36h forecasts. This figure can be compared to Figure 15 which shows the same differences for REF and TOTAL. For 2m temperature, the magnitude of the changes brought by interactive aerosol-radiation interaction is similar in the experiments with and without assimilation. This is rue for both the SW and LW dust-meteolorogy feedbacks. However, the impact on surface winds and dust production are more important with assimilation runs. This different behaviour can be explained by the fact that the time scales are different for the surface temperature and for wind speed adjustments to the radiative forcings. The heat capacity of sand is low, which makes the thermal inertia of desertic soils small as well: surface temperature adjusts quickly to a change in the radiative fluxes. As a consequence, the fact that there the analysis takes into account dust-radiation interaction from an aerosol climatology or from interactive aerosols doesn't have such a large impact, as surface temperature adjusts quickly to the radiative forcings during the forecast. However, for winds, the adjustment takes more time since the changes are driven by vertical and horizontal temperature gradients, and the changes concern the whole boundary layer (see Figure 16). As a consequence, it seems that the fact that interactive dust-radiation is taken into account in the analysis of TOTAL_ASSIM, through the first guess, enhances the feedback between radiation and surface winds as compared to TOTAL. The weight of the fist guess in the analysis is amplified by the fact that the dust storm of 17-18 April 2012 occurred in a region where both meteorological and total AOD observations are sparse.

The impact on dust production is clear : the difference between TOTAL_ASSIM and REF_ASSIM is more marked, at 0UTC and at 12UTC, than the difference between TOTAL and REF. However, the feedbacks associated with dust-SW and LW radiation interaction, even if they are more intense as compared to TOTAL, appear to attenuate the impact of each other: in the dust storm, the difference in AOD seldom exceeds 0.1 between TOTAL_ASSIM and REF_ASSIM. A few hundred of kilometers East of the storm, the impact is not negligible, with dust AOD being reduced by 0.2 to 0.3 with TOTAL_ASSIM, at 0 and 12UTC.

8.1 Impact on the quality of temperature and AOD forecasts by the MACC global system

The previous sections showed that surface temperature is significantly affected by how the aerosol radiative effect is computed. The impact on AOD is more localized but not negligible. This sections aims to assess whether using prognostic aerosols to compute the aerosol radiative effect is beneficial for the forecasts of these two parameters. As assimilation runs are considered, the configuration is very close to that of the NRT global MACC-II system.

8.1.1 Temperature forecasts

Temperature forecasts of TOTAL_ASSIM are evaluated against observations for several stations in Egypt. As the resolution was rather crude, several stations were not taken into account because of land-sea representativity problems. Figure 14 showed that using prognostic aerosols has a beneficial impact on temperature forecasts with cycling experiments: a negative bias on minimum temperatures is diminished and RMSE is decreased. In this section a more general approach is followed: forecasts are evaluated for the period from 10th to 25th of April 2012, over the whole of Egypt, for runs starting at 00UTC. Only REF_ASSIM and TOTAL_ASSIM will be assessed as they correspond to the operational setup of the MACC global system. The evaluation will be carried out for 2m temperature because it is the meteorological parameter

that was the most impacted by the interactive aerosols radiative effect and for which observations are widely available.

Tables 2 and 3 show the RMSE and bias of the REF_ASSIM and TOTAL_ASSIM, over a selection of stations in Egypt and Israel, for forecast times ranging from 0 to 48h. The analysis of 2m temperature is significantly improved both in terms of RMSE and bias, respectively up 10% and 20%. This shows that with assimilation runs, the impact of using prognostic aerosols radiative effect is important for the analysis and for short-term forecasts. 24h forecasts also show an improvement of close to 20

12 and 36h Forecasts show no improvement of TOTAL_ASSIM compared to REF_ASSIM in terms of RMSE. The bias decreases significantly for both forecast times, which leads to a small cold bias at 12h forecast, and an improvement of the warm bias at 36h forecast time.

It appears that the overall improvement brought by TOTAL_ASSIM is important for the initial conditions and forecasts of temperatures at night, and smaller during the day. The positive impact on RMSE for nocturnal temperatures appear to be smaller and smaller with forecast time. This is probably because the errors on the amount of dust and on the location/timing of the dust storm increase with forecast time. As a consequence, errors caused by the radiative impact of aerosols also grow with forecast time, which counterbalance the positive impact that the prognostic aerosols radiative impact show on the analysis and short-term forecasts.

8.1.2 AOD forecasts

Figure 18 shows the RMSE and bias of AOD forecasted by REF_ASSIM and TOTAL_ASSIM against 228 AERONET stations over the globe, as a function of forecast times. Over the globe, the interaction between aerosol and SW radiation appear to be predominant over the interaction with LW radiation, since the bias is slightly reduced by TOTAL_ASSIM. This is a improvement for forecast times up to 4 days, and a small degradation after that. The improvement in RMSE is larger than the improvement of the bias, showing that taking into account interactive aerosol-radiation interaction improves the representation of aerosols in the model. While the bias reduction increases with forecast time, the improvement in RMSE is comparable at day+5 and day+1.

9 Summary

A series of interactions between aerosols and meteorology was highlighted in this study, driven by the forcings in the short-wave and in the long-wave. In the short-wave, lower maximum temperatures increased lower atmosphere stability, which brought in turn a decrease in wind speed and in dust production through saltation processes. Locally, at the edge of the dust plume and before the cold front, the forcings in incoming solar radiation brought differentiated cooling, which increased the horizontal temperature gradient and thermal winds. As thermal wind and synoptic winds were in the same direction, this process locally increased sharply surface winds and dust production.

Thermal emissions of the dust layer brought opposite feedbacks: warmer temperatures at night decreased the stability of the PBL, thus strengthening surface winds and dust emissions. As with short-wave forcing, contrasted heating of the surface at night increased the horizontal temperature gradient at the edge of the dust plume. As the increased thermal wind and synoptic winds were in opposite directions, the consequence was locally weaker winds and dust emissions.

Assimilation runs confirmed these feedback, as they translated into the initial conditions of both aerosols and temperature. Since the considered region doesn't have much observations of both temperature and total AOD from MODIS to constrain the initial conditions, the first guess has an unusually large importance in the initial conditions. The synoptic situation wasn't much changed between REF_ASSIM and TOTAL_ASSIM. Scores on surface temperatures and on AOD showed that the forecasts were of better quality when using prognostic aerosols instead of the Tegen aerosol climatology to compute the aerosols-radiation interaction, for forecast times up to 48h.

10 Conclusions

We studied feedback effects between dust and radiation and associated changes in the meteorological parameters in the PBL with the MACC-II global system during the dust storm of 17th-19th of April 2012 in the Eastern Mediterranean. Simulations that use either the Tegen aerosol climatology or the prognostics aerosol forecast by the MACC model to compute the aerosol direct effect were compared. Dust aerosols were shown to have significant impact on downward radiative fluxes, reducing the short-wave component and increasing the long-wave one. That radiative impact affected in turn surface temperature, and thus lower atmosphere stability. This in turn led to local increases or decreases in wind speeds and dust production. Overall, for this situation, the dust-radiation interaction on the long-wave spectrum and the in the short-wave spectrum both had a strong impact on atmospheric stability and dust production. This highlights how important accurate forecasts of the timing of the storm are, since depending on the local time of the dust lifting episodes, the interaction between aerosol and boundary layer meteorology are of a very different nature.

Compared against observations, downward radiative fluxes, especially in the long-wave spectrum, are better forecasted in this situation when using interactive aerosols to compute the aerosol-radiation interaction. Surface temperatures and dust AOD itself were better forecasted for short-term forecasts, as the aerosol plume is by then forecasted with a relatively small error. For larger forecast times, the

fact that errors in the prediction of the location and timing of aerosol layers are larger can make the prognostic aerosol direct effect have a negative impact. There exist however alternatives between full prognostic aerosol direct effect and climatological aerosol direct effect. Prognostic aerosol direct effect can be used only in the short forecast that is used as the first guess in the assimilation step for example, thus bringing an improvement in the aerosol and temperatures analysis. Prognostic aerosol direct effect could also be relaxed towards climatological aerosol direct effect, depending on the forecast time.

Acknowledgements. We thank NASA for providing the MODIS data, and the AERONET and BSRN projects for making their data freely and easily available. The authors also wish to thank Robin Hogan for his useful suggestions. This research was supported by the EU Seventh Research Framework Programme (MACC-II project, contract number 283576).

References

Banta, R.M., Newsom, R.K., Lundquist, J.K., Pichugina, Y.L., Coulter, R.L. and L. Mahrt L: Nocturnal low-level het characteristics over Kansas during CASES-99, Boundary Layer Meteorology, 105, 2, 221-252, 2002.

Bellouin, N., Boucher, O., Haywood, J. and Shekar Reddy, M.: Global estimate of aerosol direct radiative forcing from satellite measurements, Nature, 438, 1138-1141, 2005.

Benedetti, A., Morcrette, J.-J., Boucher, O., Dethof, A., Engelen, R.J., Fisher, M., Flentje, H., Huneeus, N., Jones, L., Kaiser, J.W., Kinne, S., Mangold, A., Razinger, M., Simmons, A.J. and Suttie, M., Aerosol analysis and forecast in the European Centre for Medium-Range Weather Forecasts Integrated Forecast System: 2. Data assimilation, J. Geophys. Res., 114, D13205, doi:10.1029/2008JD011115.

Boucher, O., Pham, M. and C. Venkataraman, Simulation of the atmospheric sulfur cycle in the LMD GCM: Model description, model evaluation, and global and European budgets, Note 23, 26 pp., Inst. Pierre-Simon Laplace, Paris, France, 2002.

Choi, J.-O. and Chung, C.-E.: Sensitivity of aerosol direct radiative forcing to aerosol vertical profile, Tellus B 2014, 66, 24376, doi:http://dx.doi.org/10.3402/tellusb.v66.24376, 2014.

Fiedler S., Schepanski K., Heinold B., Knippertz P. and I. Tegen: Climatology of nocturnal low-level jets over North Africa and implications for modeling mineral dust emission. J Geophys Res - Atmos 118, DOI 10.1002/jgrd.50394, 2013.

Ginoux, P., M. Chin, I. Tegen, J. Prospero, B. N. Holben, O. Dubovik, and S.-J. Lin, Sources and distributions of dusts simulated with the GOCART model, J. Geophys. Res., 106, 20,255 – 20,274, 2001.

Haywood, J. M., Osborne, S. R., Francis, P. N., Kiel, A., Formenti, P., Andreae, M. O., and Kaye, P. H.: The mean physical and optical properties of regional haze dominated by biomass burning aerosol measured from the C-130 aircraft during SAFARI 2000, J. Geophys. Res., 108, 8473, doi:10.1029/2002JD002226, 2003.

Heimo, A., Vernez, A., and Wasserfallen, P. (1993), Baseline Surface Radiation Network (BSRN). Concept and Implementation of a BSRN Station, WMO/td-no. 579, World Meteorological Organization,Geneva, Switzerland.

Heinold A., Tegen, I., Schepanski, I. and Hellmuth, O.: Dust radiative feedback on Saharan boundary layer dynamics and dust mobilization, Geophys. Res. Letters, 35, 20, L20817, doi:10.1029/2008GL035319, 2008.

Heinold B., Knippertz P., Marsham J.H., Fiedler S., Dixon N.S., Schepanski K., Laurent B. and I. Tegen: The role of deep convection and nocturnal low-level jets for dust emission in summertime West Africa: Estimates from convection-permitting simulations. J Geophys Res - Atmos 118:1-16, DOI 10.1002/jgrd.50402, 2013.

Heinold, B., Knippertz, P. and Beare, R. J. (2014), Idealized large-eddy simulations of nocturnal low-level jets over subtropical desert regions and implications for dust-generating winds. Q.J.R. Meteorol. Soc.. doi: 10.1002/qj.2475

Holben B.N., T.F. Eck, I. Slutsker, D. Tanré, J.P. Buis, A. Setzer, E. Vermote, J.A. Reagan, Y. Kaufman, T. Nakajima, F. Lavenu, I. Jankowiak, and A. Smirnov, 1998: AERONET - A federated instrument network and data archive for aerosol characterization, Rem. Sens. Environ., 66, 1-16.

Hollingsworth, A., Engelen, R. J., Textor, C., Benedetti, A., Boucher, O., Chevallier, F., Dethof, A., Elbern, H., Eskes, H., Flemming, J., Granier, C., Kaiser, J. W., Morcrette, J.-J., Rayner, P., Peuch, V.-H., Rouil, L., Schultz, M. G., and Simmons, A. J.: Toward a Monitoring and Forecasting System For Atmospheric Composition: The GEMS Project, Bull. Am. Meteor. Soc., 89, 1147–1164, 2008.

Holton, James R. (2004). An Introduction to Dynamic Meteorology. New York: Academic Press. ISBN 0-12-354015-1.

Hoose, C. and Möhler, O.: Heterogeneous ice nucleation on atmospheric aerosols: a review of results from laboratory experiments, Atmos. Chem. Phys., 12, 9817-9854, doi:10.5194/acp-12-9817-2012, 2012.

Huneeus, N., Schulz, M., Balkanski, Y., Griesfeller, J., Prospero, J., Kinne, S., Bauer, S., Boucher, O., Chin, M., Dentener, F., Diehl, T., Easter, R., Fillmore, D., Ghan, S., Ginoux, P., Grini, A., Horowitz, L., Koch, D., Krol, M. C., Landing, W., Liu, X., Mahowald, N., Miller, R., Morcrette, J.-J., Myhre, G., Penner, J., Perlwitz, J., Stier, P., Takemura, T., and Zender, C. S.: Global dust model intercomparison in AeroCom phase I, Atmos. Chem. Phys., 11, 7781-7816, doi:10.5194/acp-11-7781-2011, 2011.

Inness, A., Baier, F., Benedetti, A., Bouarar, I., Chabrillat, S., Clark, H., Clerbaux, C., Coheur, P., Engelen, R. J., Errera, Q., Flemming, J., George, M., Granier, C., Hadji-Lazaro, J., Huijnen, V., Hurtmans, D., Jones, L., Kaiser, J. W., Kapsomenakis, J., Lefever, K., Leitão, J., Razinger, M., Richter, A., Schultz, M. G., Simmons, A. J., Suttie, M., Stein, O., Thépaut, J.-N., Thouret, V., Vrekoussis, M., Zerefos, C., and the MACC team: The MACC reanalysis: an 8-yr data set of atmospheric composition, Atmos. Chem. Phys. Discuss., 12, 31247-31347, doi:10.5194/acpd-12-31247-2012, 2012.

Boucher, O., D. Randall, P. Artaxo, C. Bretherton, G. Feingold, P. Forster, V.-M. Kerminen, Y. Kondo, H. Liao, U. Lohmann, P. Rasch, S.K. Satheesh, S. Sherwood, B. Stevens and X.Y. Zhang, 2013. [Stocker, T.F., D. Qin, G.-K. Plattner, M. Tignor, S.K. Allen, J. Boschung, A. Nauels, Y. Xia, V. Bex and P.M. Midgley (eds.)].Cambridge University Press, Cambridge, United Kingdom and New York, NY, USA.

Kamal, M.M., Qu, J.J. and Hao, X.: A Study of Dust Aerosols Impact on Hurricanes with Multi-Sensors Measurement from Space, The Open Remote Sensing Journal, 5, 73-82, 2012.

Knippertz P.: Dust emissions in the West African heat trough: the role of the diurnal cycle and of extratropical disturbances. Meteorologische Zeitschrift 17(5):553-563, DOI: 10.1127/0941-2948/2008/0315 ,2008.

Koch, D. and Del Genio, A. D.: Black carbon semi-direct effects on cloud cover: review and synthesis, Atmos. Chem. Phys., 10, 7685-7696, doi:10.5194/acp-10-7685-2010, 2010.

Lyubansky, V. (2012): Meteorological synoptical observations from station Sede Boqer (2012-01). The Jacob Blaustein Institutes for Desert Research, Sede Boqer, doi:10.1594/PANGAEA.802681

Marticorena, B. and G. Bergametti: Modeling the atmospheric dust cycle: 1. Design of a soil-derived dust emission scheme, J. Geophys. Res., 100, 2156-2202, DOI: 10.1029/95JD00690, 1995.

Mimouni, M.: Basic measurements of radiation at station Tamanrasset (2013-09). National Meteorological Office of Algeria, doi:10.1594/PANGAEA.822372, 2013

Miller, R.L., P. Knippertz, C. Pérez García-Pando, J.P. Perlwitz, and I. Tegen: Impact of dust radiative forcing upon climate. In Mineral Dust: A Key Player in the Earth System. P. Knippertz, and J.-B.W. Stuut, Eds. Springer, 327-357, doi:10.1007/978-94-017-8978-3_13, 2014.

Morcrette, J.-J., Boucher, O., Jones, L., Salmond, D., Bechtold, B., Beljaars, A., Benedetti, A., Bonet, A., Kaiser, J.W., Razinger, M., Schulz, M., Serrar, S., Simmons, A.J., Sofiev, M., Suttie, M., Tompkins, A.M. and Untch, A. (2009), Aerosol analysis and forecast in the European Centre for Medium-Range Weather Forecasts Integrated Forecast System: Forward modeling, J. Geophys. Res., 114, D06206, doi:10.1029/2008JD011235.

Mulcahy, J. P., Walters, D. N., Bellouin, N., and Milton, S. F.: Impacts of increasing the aerosol complexity in the Met Office global numerical weather prediction model, Atmos. Chem. Phys., 14, 4749-4778, 2014.

Nickovic, S., G. Kallos, A. Papadopoulos, and O. Kakaliagou (2001), A model for prediction of desert dust cycle in the atmosphere, J. Geophys. Res., 106(D16), 18113–18129, doi:10.1029/2000JD900794.

Niemand, M., Möhler, O., Vogel, B., Vogel, H., Hoose, C., Connolly, P., Klein, H., Bingemer, H., DeMott, P., Skrotzki, J. and T. Leisner: A Particle-Surface-Area-Based Parameterization of Immersion Freezing on Desert Dust Particles. J. Atmos. Sci., 69, 3077–3092, doi: http://dx.doi.org/10.1175/JAS-D-11-0249.1, 2012.

Painemal, D. and Zuidema, P.: The first aerosol indirect effect quantified through airborne remote sensing during VOCALS-REx, Atmos. Chem. Phys., 13, 917-931.

Pérez, C., S. Nickovic, G. Pejanovic, J.M. Baldasano, and E. Özsoy: Interactive dust-radiation modeling: A step to improve weather forecast. J. Geophys. Res., 111, D16206, doi:10.1029/2005JD006717, 2006.

Peuch, V.-H. and Engelen, R.J.: Towards and operational GMES Atmosphere Monitoring Service, ECMWF Newsletter No. 132, 20-25, 2012.

Reale, Oreste, K. M. Lau, Arlindo da Silva, 2011: Impact of Interactive Aerosol on the African Easterly Jet in the NASA GEOS-5 Global Forecasting System. Wea. Forecasting, 26, 504–519.

Reddy, M. S., Boucher, O., Bellouin, N., Schulz, M., Balkanski, Y., Dufresne J.-L. and M. Pham, Estimates of global multicomponent aerosol optical depth and direct radiative perturbation in the Laboratoire de Meteorologie Dynamique general circulation model, J. Geophys. Res., 110, D10S16, doi:10.1029/2004JD004757, 2005.

Rodwell, M. J. and Jung, T.: Understanding the local and global impacts of model physics changes: an aerosol example, Q.J.R.Meteorol. Soc., 134, 1479–1497, 2008.

Schulz, M., C. Textor, S. Kinne, Y. Balkanski, S. Bauer, T. Berntsen, T. Berglen, O. Boucher, F. Dentener, A. Grini, S. Guibert, T. Iversen, D. Koch, A. Kirkevåg, X. Liu, V. Montanaro, G. Myhre, J. Penner, G. Pitari, S. Reddy, O. Seland, P. Stier, and T. Takemura: Radiative forcing by aerosols as derived from the AeroCom present-day and pre-industrial simulations, Atmos. Chem. Phys., 6, 5225-5246, 2006.

Shi, Y; Zhang, J; Reid, JS; Hyer, EJ; Hsu, NC: Critical evaluation of the MODIS Deep Blue aerosol optical depth product for data assimilation over North Africa. ATMOSPHERIC MEASUREMENT TECHNIQUES, 6(4), 949-969, 2013.

Spyrou, C., Kallos, G., Mitsakou, C., Athanasiadis, P., Kalogeri, C., and Iacono, M. J.: Modeling the radiative effects of desert dust on weather and regional climate, Atmos. Chem. Phys., 13, 5489-5504, doi:10.5194/acp-13-5489-2013, 2013.

Stanelle, T., Vogel, B., Vogel, H., Bäumer, D., and Kottmeier, C.: Feedback between dust particles and atmospheric processes over West Africa during dust episodes in March 2006 and June 2007, Atmos. Chem. Phys., 10, 10771-10788, doi:10.5194/acp-10-10771-2010, 2010.

Stengel, M.; Kniffka, A.; Meirink, J.F.; Riihelä, A.; Trentmann, J.; Müller, R.; Lockhoff, M.; Hollmann, R. (2013): CLAAS: CM SAF CLoud property dAtAset using SEVIRI - Edition 1 - Hourly / Daily Means, Pentad Means, Monthly Means / Monthly Mean Diurnal Cycle / Monthly Histograms. Satellite Application Facility on Climate Monitoring. DOI:10.5676/EUM_SAF_CM/CLAAS/V001

Stier, P., Schutgens, N. A. J., Bellouin, N., Bian, H., Boucher, O., Chin, M., Ghan, S., Huneeus, N., Kinne, S., Lin, G., Ma, X., Myhre, G., Penner, J. E., Randles, C. A., Samset, B., Schulz, M., Takemura, T., Yu, F., Yu, H., and Zhou, C.: Host model uncertainties in aerosol radiative forcing estimates: results from the AeroCom Prescribed intercomparison study, Atmos. Chem. Phys., 13, 3245-3270, doi:10.5194/acp-13-3245-2013, 2013

Sun, Y. L., Wang, Z. F., Fu, P. Q., Yang, T., Jiang, Q., Dong, H. B., Li, J., and Jia, J. J.: Aerosol composition, sources and processes during wintertime in Beijing, China, Atmos. Chem. Phys., 13, 4577-4592, doi:10.5194/acp-13-4577-2013, 2013.

egen, I., and A.A. Lacis: Modeling of particle size distribution and its influence on the radiative properties of mineral dust aerosol. J. Geophys. Res., 101, 19237-19244, doi:10.1029/95JD03610, 1996.

Tegen, I., P. Hoorig, M. Chin, I. Fung, D. Jacob, and J. Penner (1997), Contribution of different aerosol species to the global aerosol extinction optical thickness: Estimates from model results, J. Geophys. Res.,102,23,895–23,915

Tompkins, A. M., Cardinali, C., Morcrette, J. J., and Rodwell, M.: Influence of aerosol climatology on forecasts of the African Easterly Jet, Geophys. Res. Lett., 32, L10801, doi: 10.1029/2004GL022189, 2005.

Van de Wiel B., Moene A., Steeneveld G., Baas P., Bosveld F., Holtslag A.:A Concep- tional view on Inertial Oscillations and Nocturnal Low-Level Jets. J Atmos Sci 67:2679-2689, doi: http://dx.doi.org/10.1175/2010JAS3289.1, 2010.

S. Woodward: Modeling the atmospheric life cycle and radiative impact of mineral dust in the Hadley Centre climate model, J. Geophys. Res., vol. 106, No. D16, p.18,155, DOI: 10.1029/2000JD900795, 2001.

Yu, H., Kaufman, Y. J., Chin, M., Feingold, G., Remer, L. A., Anderson, T. L., Balkanski, Y., Bellouin, N., Boucher, O., Christopher, S., DeCola, P., Kahn, R., Koch, D., Loeb, N., Reddy, M. S., Schulz, M., Takemura, T., and Zhou, M.: A review of measurement-based assessments of the aerosol direct radiative effect and forcing, Atmos. Chem. Phys., 6, 613-666, doi:10.5194/acp-6-613-2006, 2006.

Yu, H., M. Chin, T. Yuan, H. Bian, L. A. Remer, J. M. Prospero, A. Omar, D. Winker, Y. Yang, Y. Zhang, Z. Zhang, and C. Zhao, The fertilizing role of African dust in the Amazon rainforest: A first multiyear assessment based on data from Cloud-Aerosol Lidar and Infrared Pathfinder Satellite Observations. Geophys. Res. Lett., 42, 1984–1991. doi: 10.1002/2015GL063040, 2015.

Zhang, J. K., Sun, Y., Liu, Z. R., Ji, D. S., Hu, B., Liu, Q., and Wang, Y. S.: Characterization of submicron aerosols during a serious pollution month in Beijing (2013) using an aerodyne high-resolution aerosol mass spectrometer, Atmos. Chem. Phys. Discuss., 13, 19009-19049, doi:10.5194/acpd-13-19009-2013, 2013.

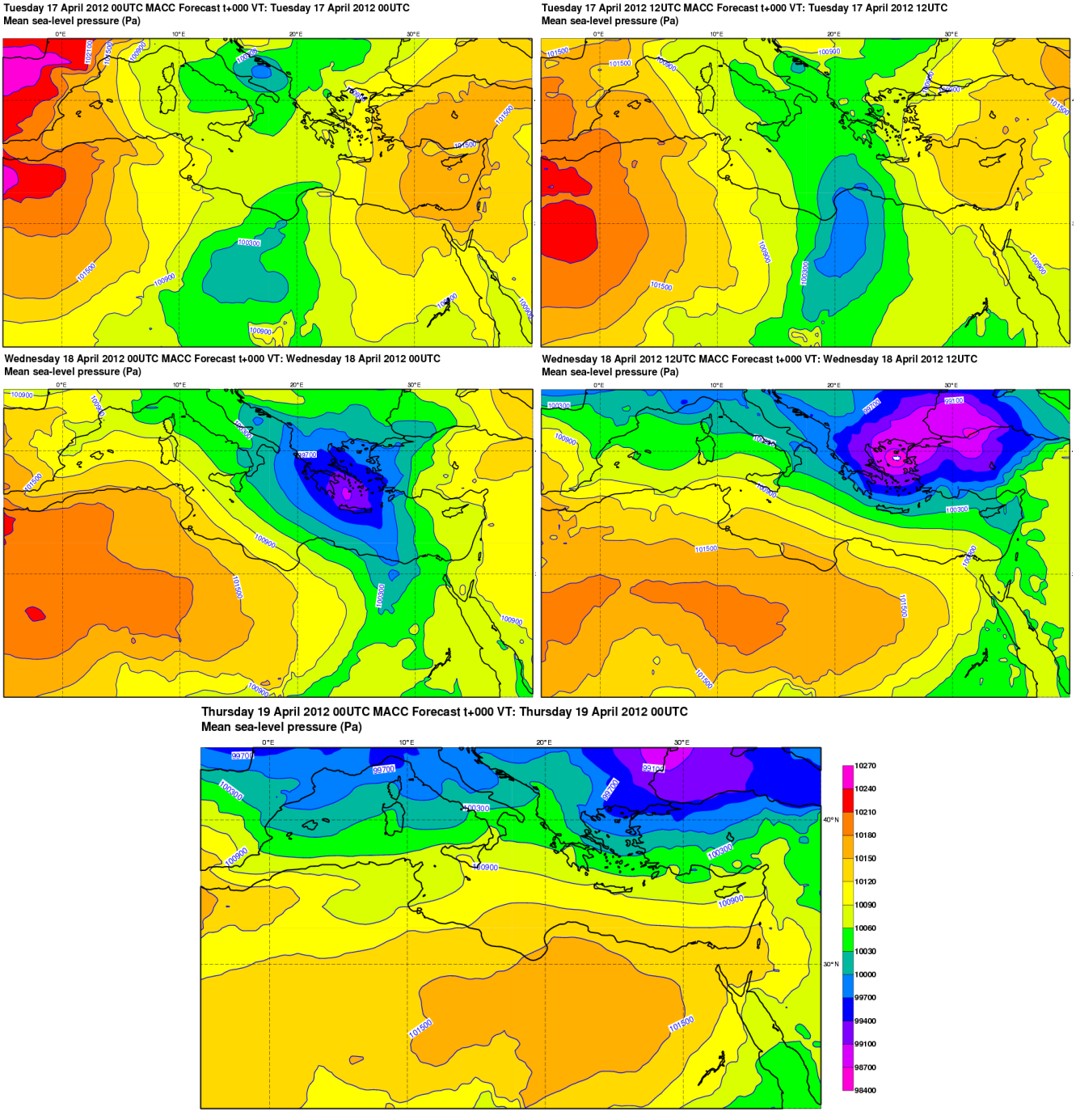

Fig. 1. Analysis of mean sea-level pressure over Northern Sahara and Southern Mediterranean from 17 April 2012 00UTC to 19th of April 2012 00UTC.

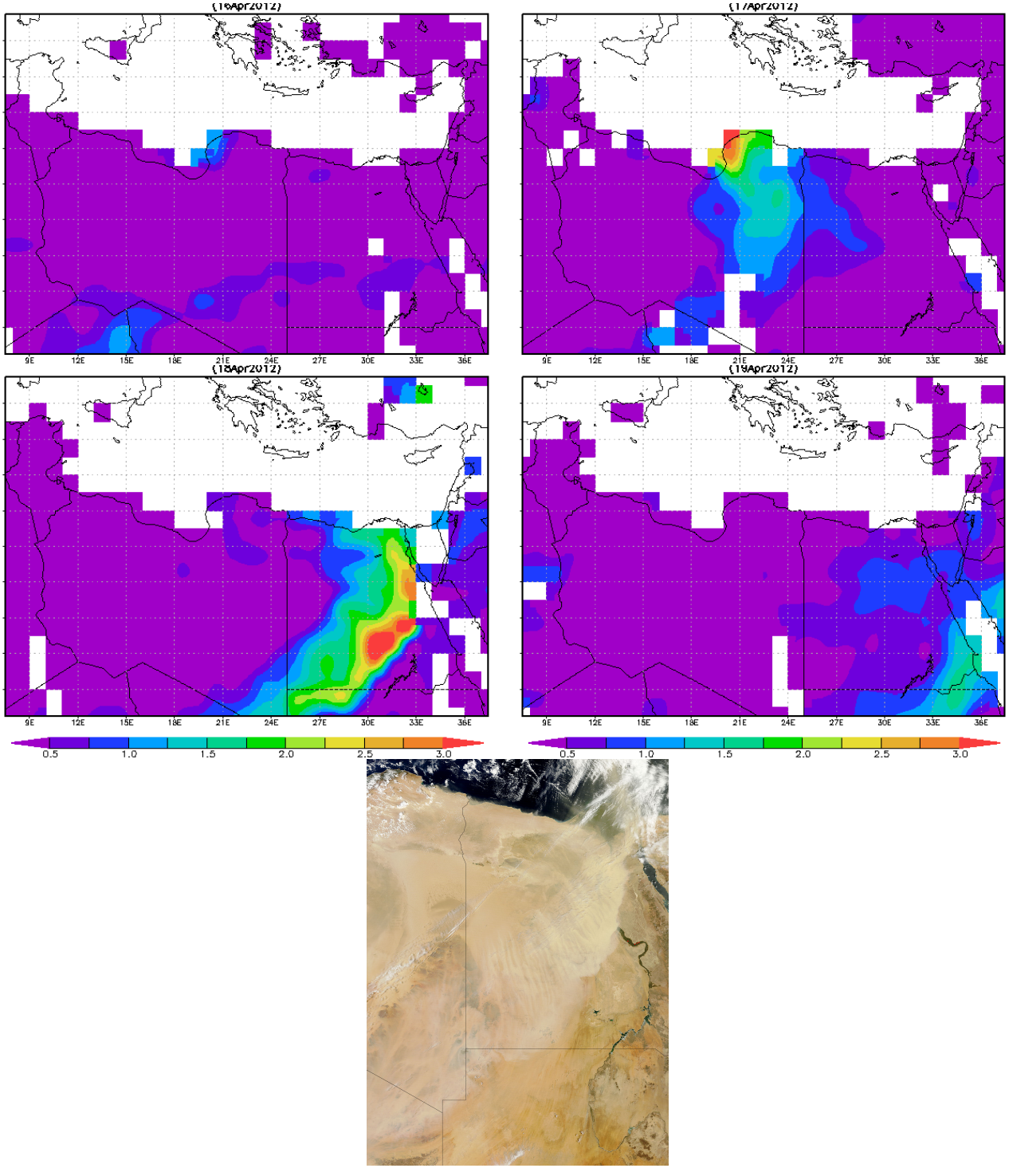

Fig. 2. AOD at 550nm from MODIS on Aqua, deep blue algorithm, daily average for 16th, 17th, 18th and 19th of April 2012. On the bottom, visible image from MODIS/Terra acquired on 18 April 2012 at 9h local time. Source http://modis.gsfc.nasa.gov/gallery/individual.php?db_date=2012-04-22

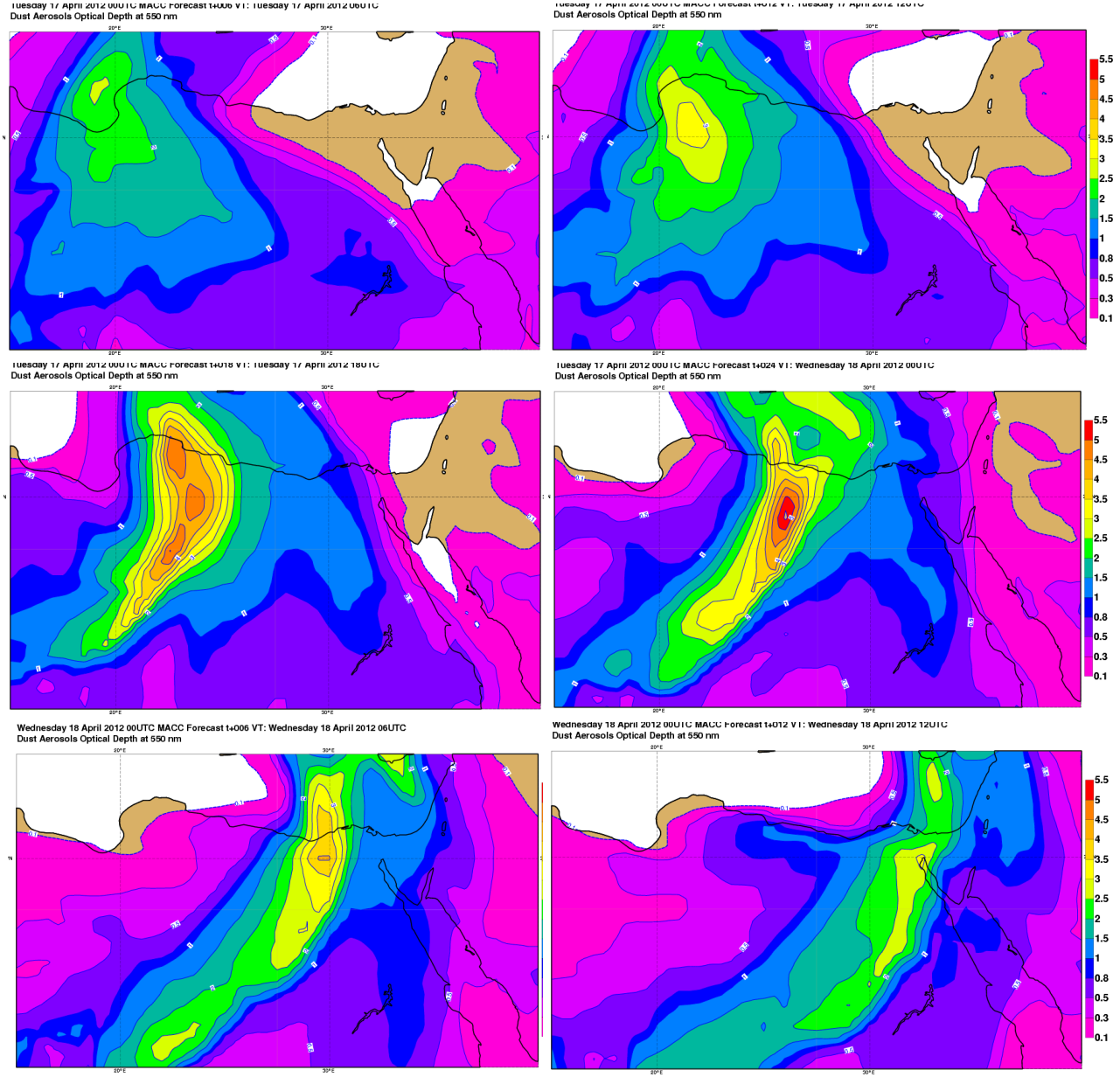

Fig. 3. AOD at 550nm from 17 April 2012 6 UTC (top left) to 18 April 12 UTC (bottom right), REF experiment starting on 17 April 2012 0UTC and 18 April 2012 0UTC.

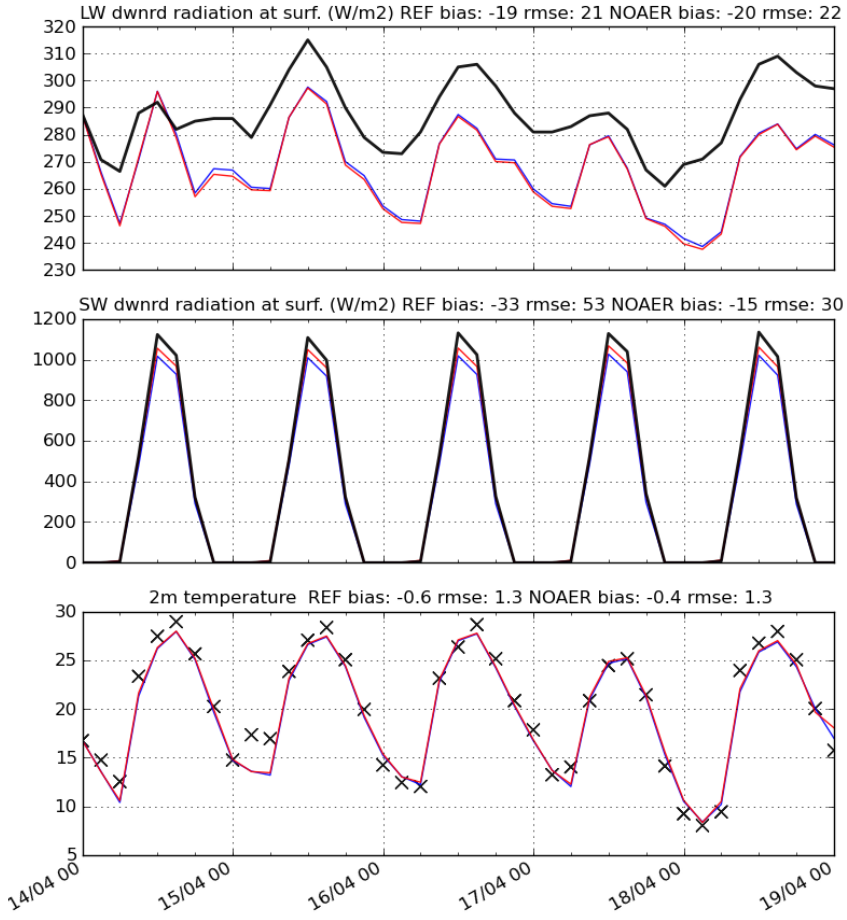

Fig. 4. 3 to 24h forecasts and observations of downward short-wave, long-wave radiation fluxes at the surface and 2m temperature at Tamanrasset. REF experiment is in blue, NOAER is in red, observations in black. The bias and RMSE of forecasts against observations for the whole period is also indicated on top.

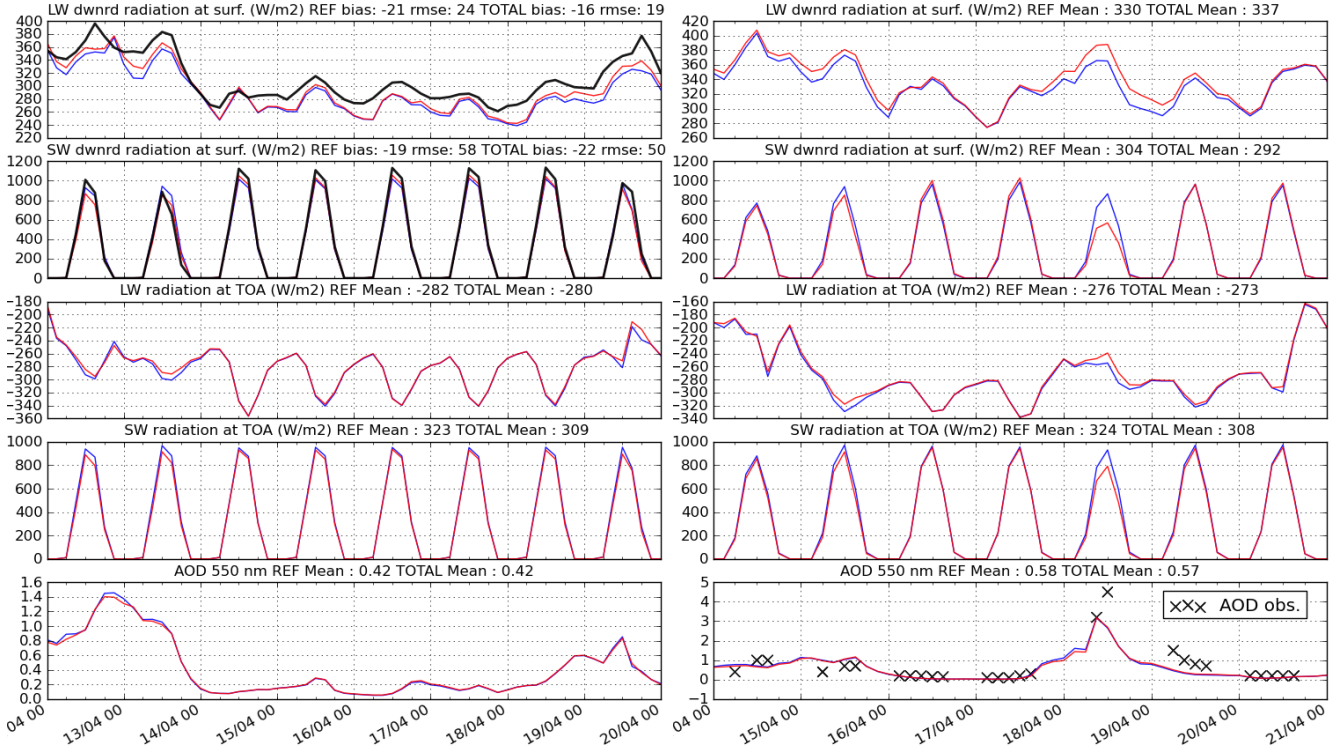

Fig. 5. 3 to 24h forecasts and observations (when available, in black) of downward short-wave and long-wave radiation fluxes at the surface and 550nm AOD at Tamanrasset (left) and Cairo (right). REF experiment is in blue, TOTAL is in red, observations in black. The bias and RMSE of forecasts against observations for the whole period is also indicated on top.

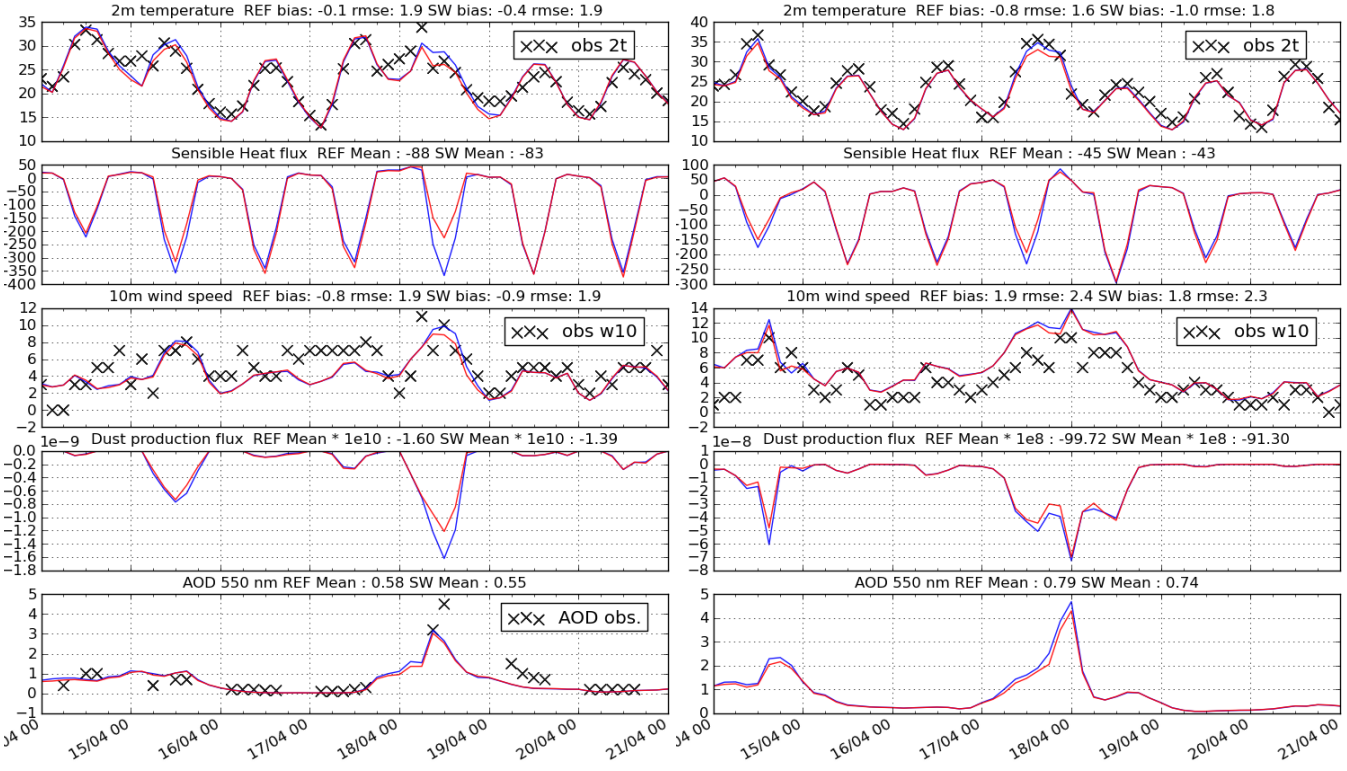

Fig. 6. REF vs SW experiment, 3 to 24h forecasts and observations of 2m temperature (in °c), sensible heat flux (in W/m^2), 10m wind speed (in m/s), dust production flux (in kg/m^2.s) and AOD at 550nm. Figures at Cairo are on the left panel and at Siwa Oasis on the right.

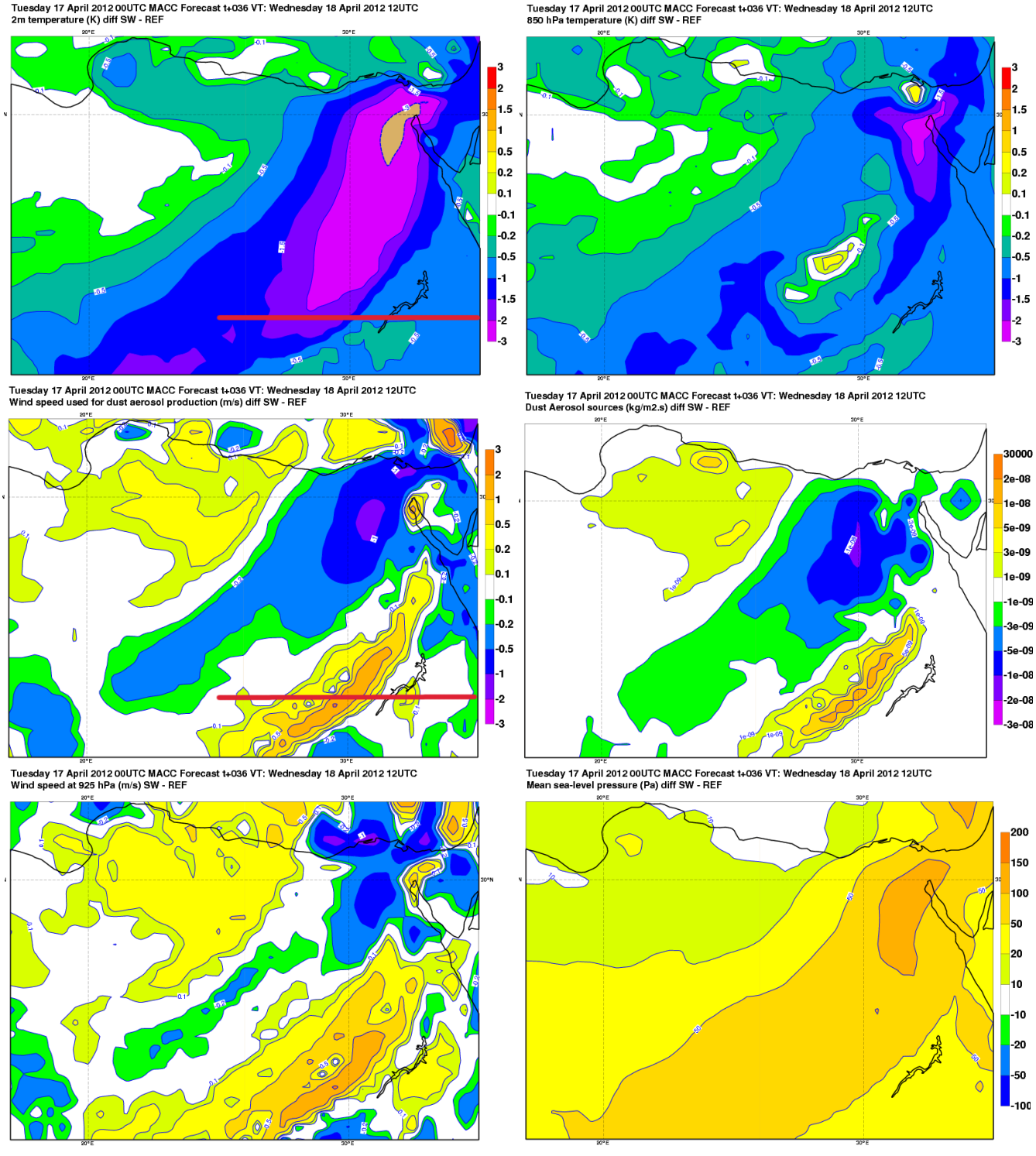

Fig. 7. Simulations starting on 17 April 2012, 36h forecast. Difference of SW - REF for 2m temperature (top left), 850 hPa temperature (top right), 10m wind speed (middle left), dust production (middle right), wind at 925 hPa (bottom left), sea-level pressure (bottom right). The red line on the 10m wind speed and 2m temperature panels indicate the cross-section of Figure 9.

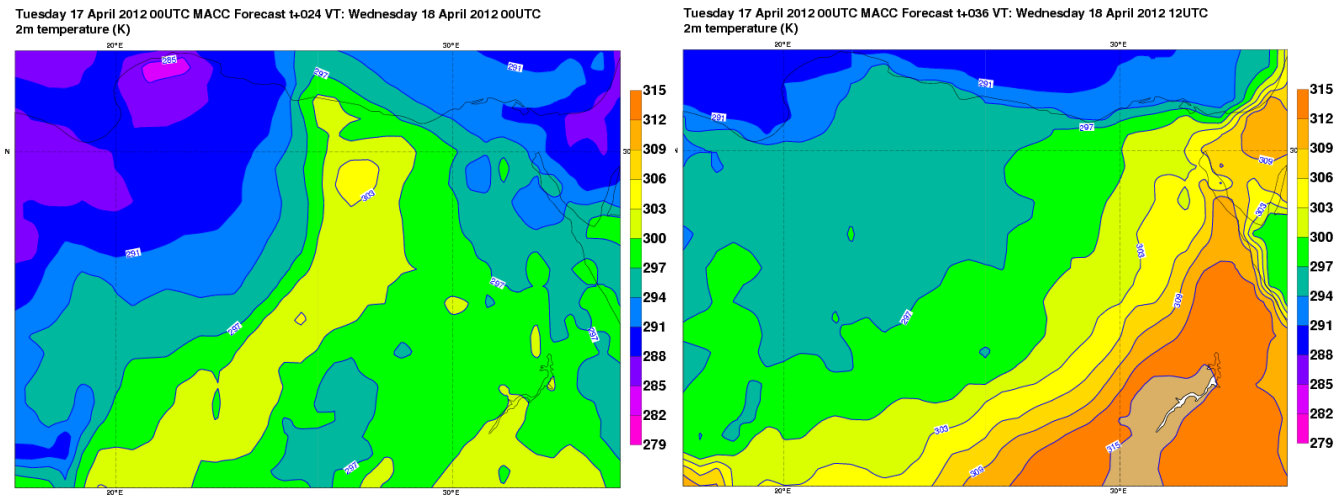

Fig. 8. Simulation starting on 17 April 2012. REF experiment for 2m temperature, 24h forecast time (left), 36h forecast time (right).

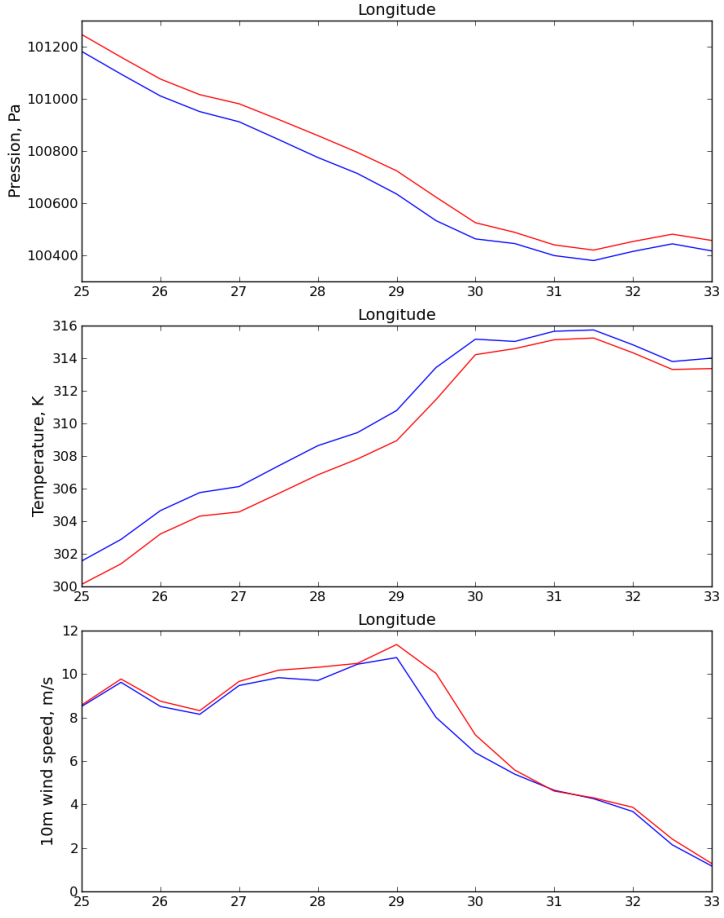

Fig. 9. Simulations starting on 17 April 2012, 36h forecast, cross-section at 22°N . Mean sea-level pressure (top), 2m temperature (middle) and 10m wind speed (bottom) for REF (blue) and SW (red).

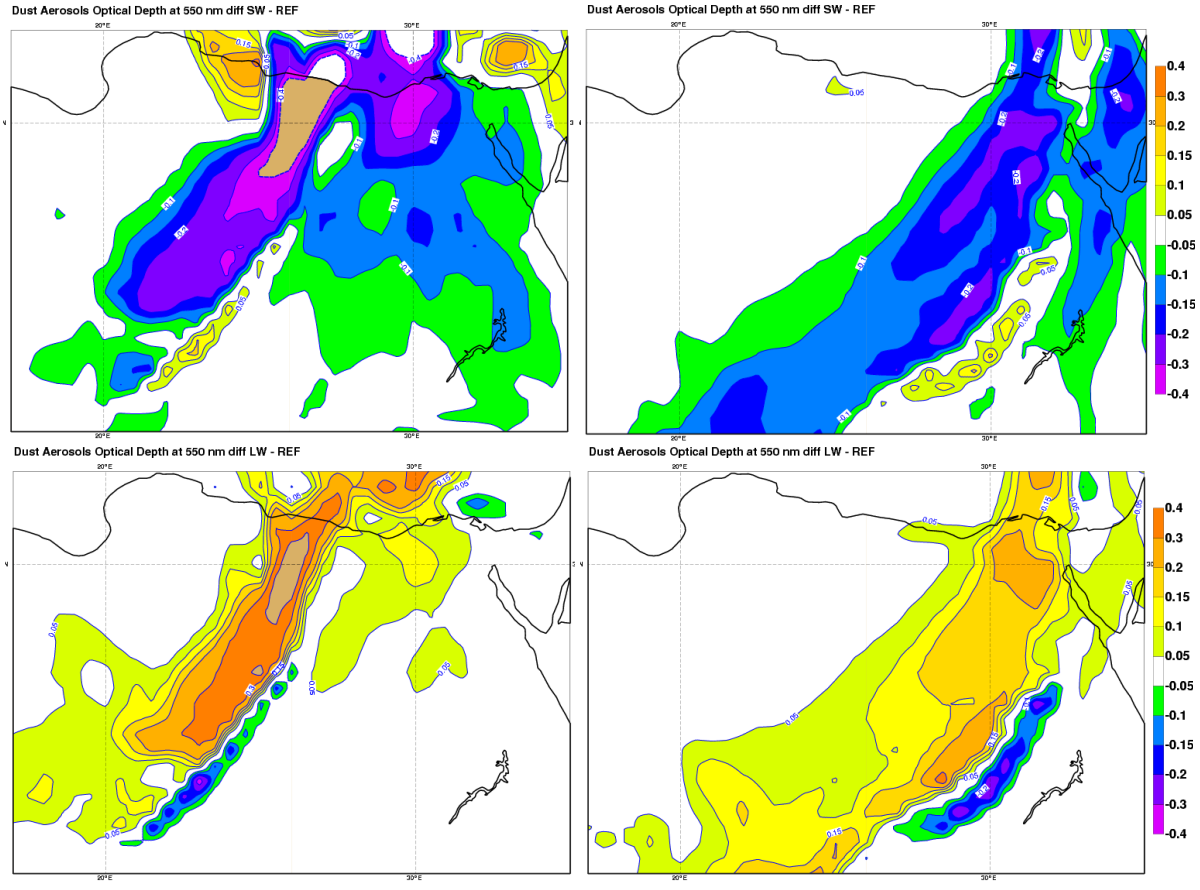

Fig. 10. Simulations starting on 17 April 2012, 24h forecast (left) and 36h (right) forecast time. Difference of AOD at 550nm, SW - REF (top), LW - REF (bottom) .

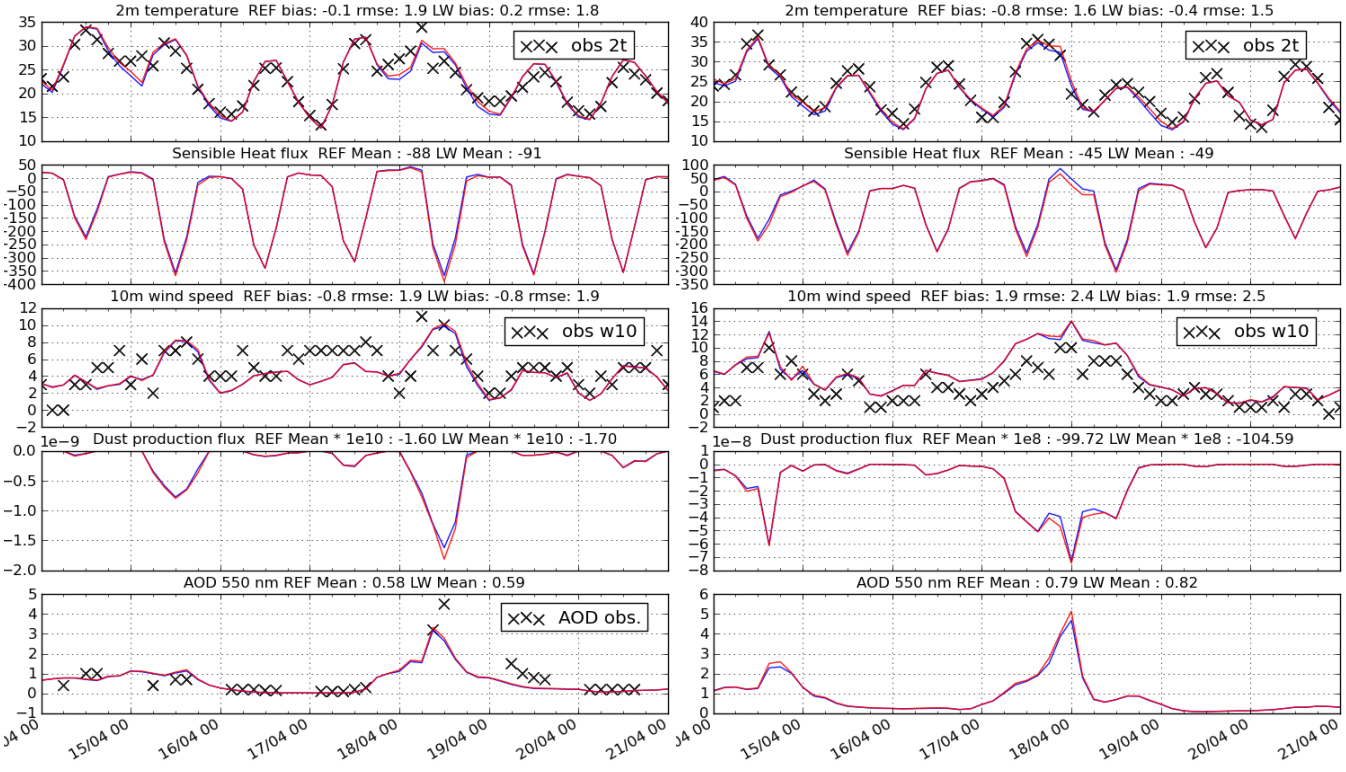

Fig. 11. Same as Figure 6 for REF vs LW experiments.

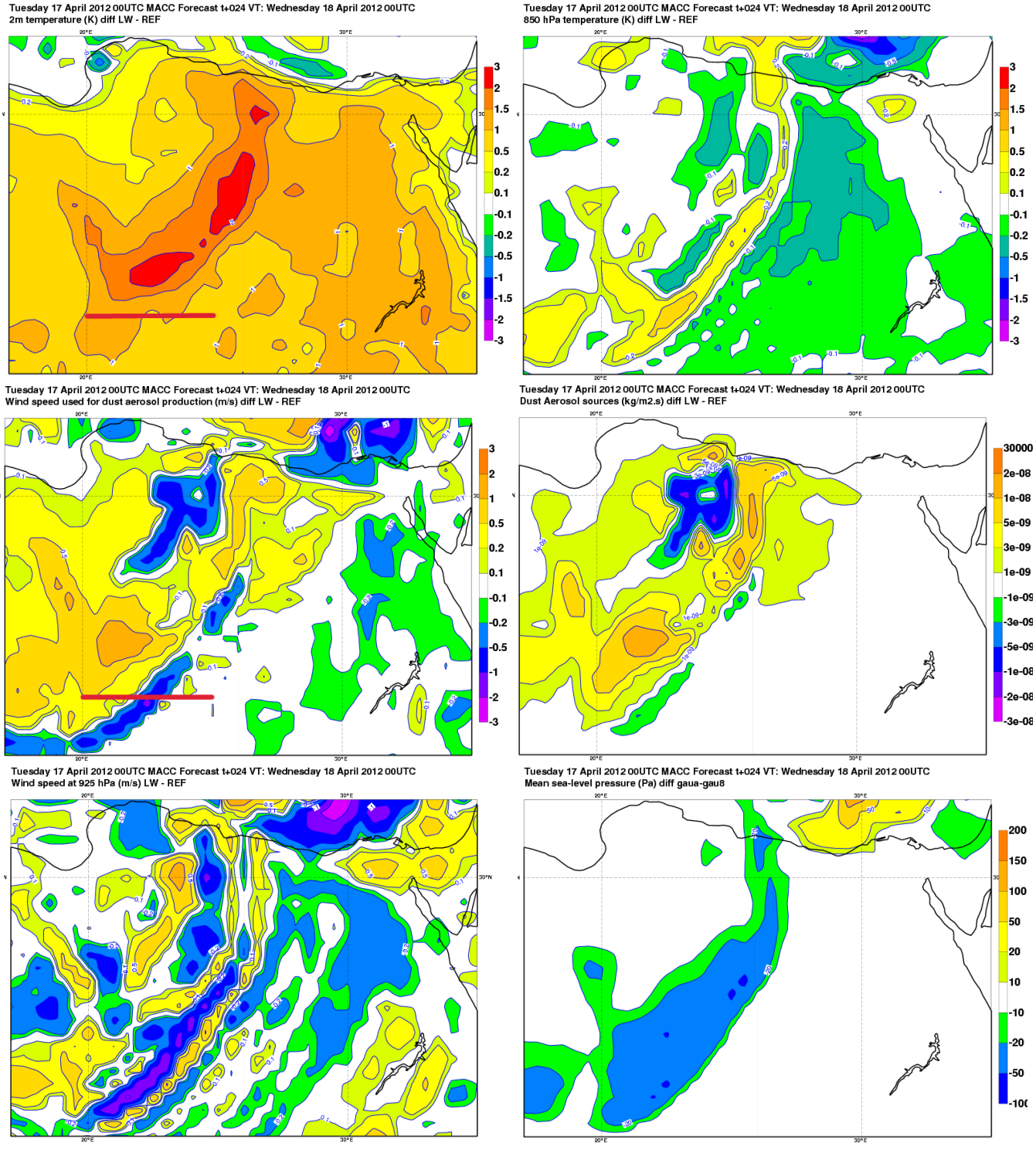

Fig. 12. Simulations starting on 17 April 2012, 24h forecast. Difference of LW - REF for 2m temperature (top left), 850 hPa temperature (top right), 10m wind speed (middle left), dust production (middle right), wind at 925 hPa (bottom left), sea-level pressure (bottom right). The red line on the 10m wind speed and 2m temperature panels indicate the cross-section of Figure 14

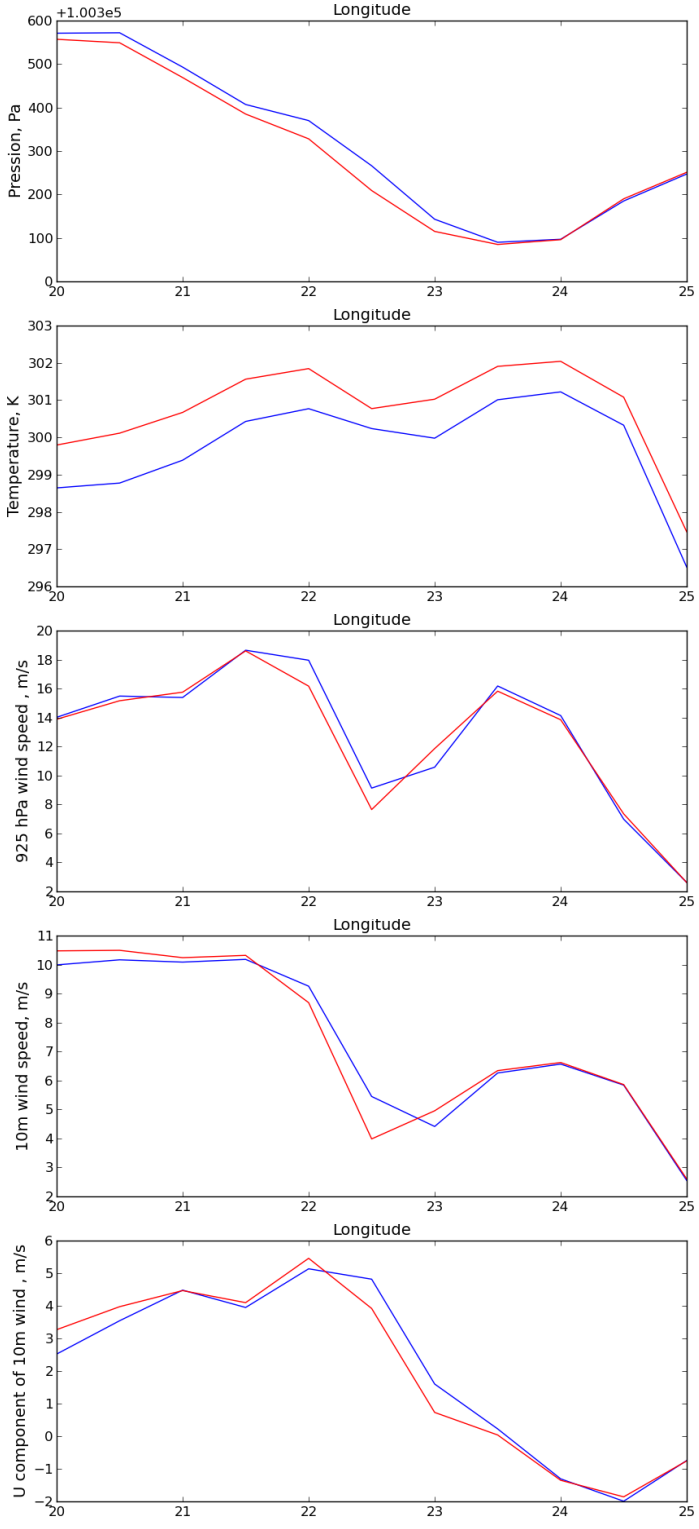

Fig. 13. Simulations starting on 17 April 2012, 24h forecast, cross-section at 22 °N . Mean sea-level pressure (top), 2m temperature (middle top), 925 hPa wind speed (middle), 10m wind speed (middle bottom) and U component of 10m wind (bottom) for REF (blue) and LW (red).

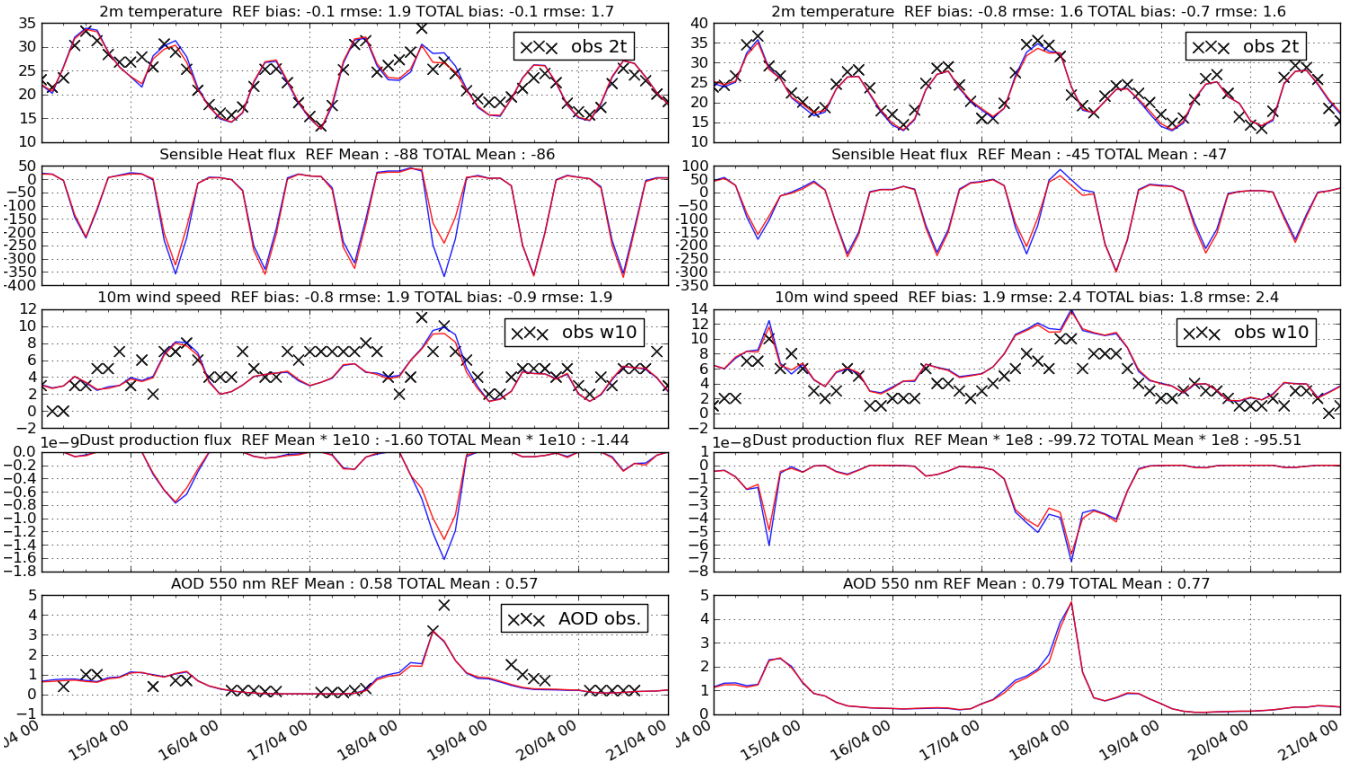

Fig. 14. Same as Figure 6 for REF vs TOTAL experiments.

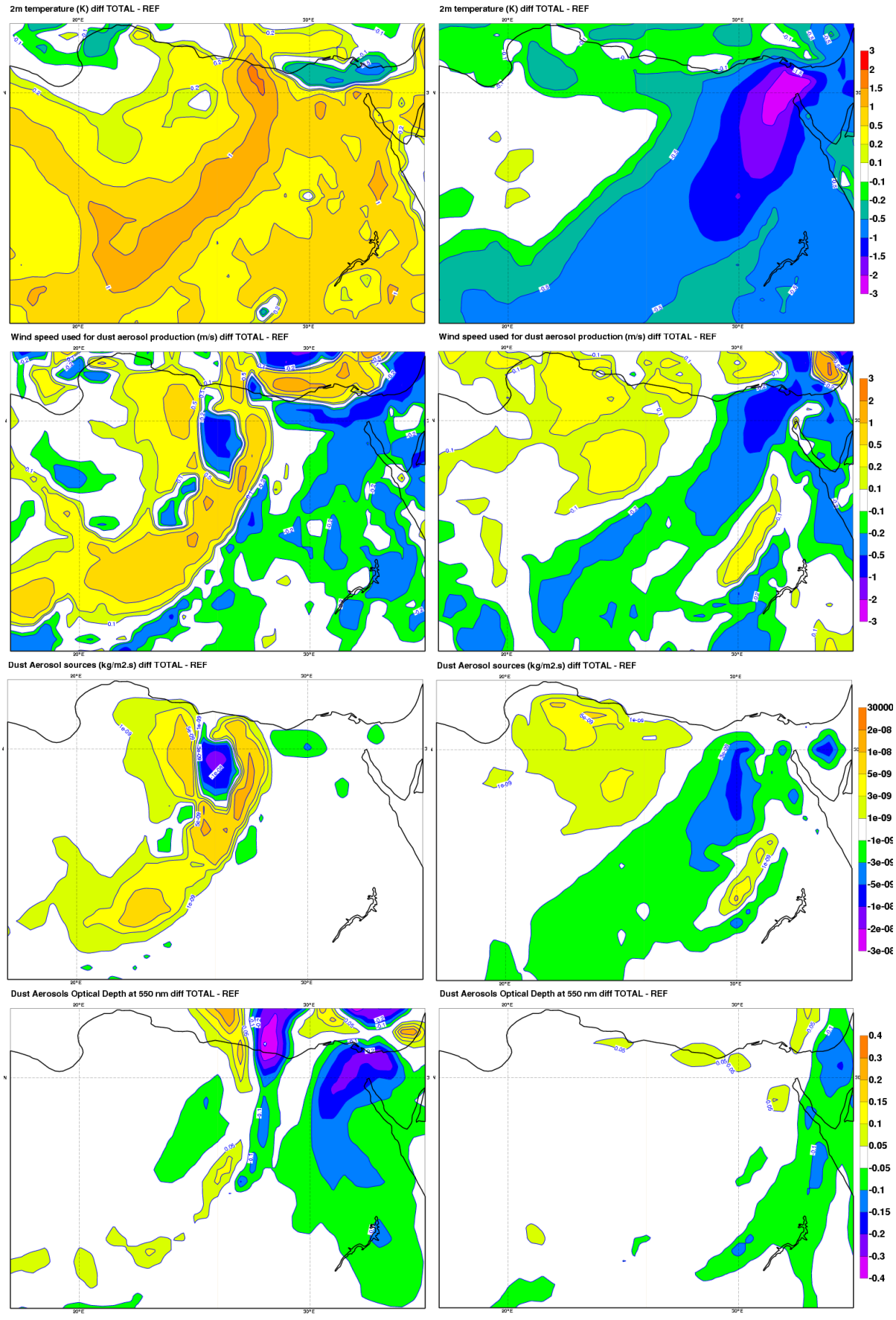

Fig. 15. Simulations starting on 17 April 2012, 24h forecast (left) and 36h (right) forecast time. Difference of TOTAL - REF for 2m temperature (top), 10m wind speed (middle top), dust production (middle bottom), dust AOD (bottom).

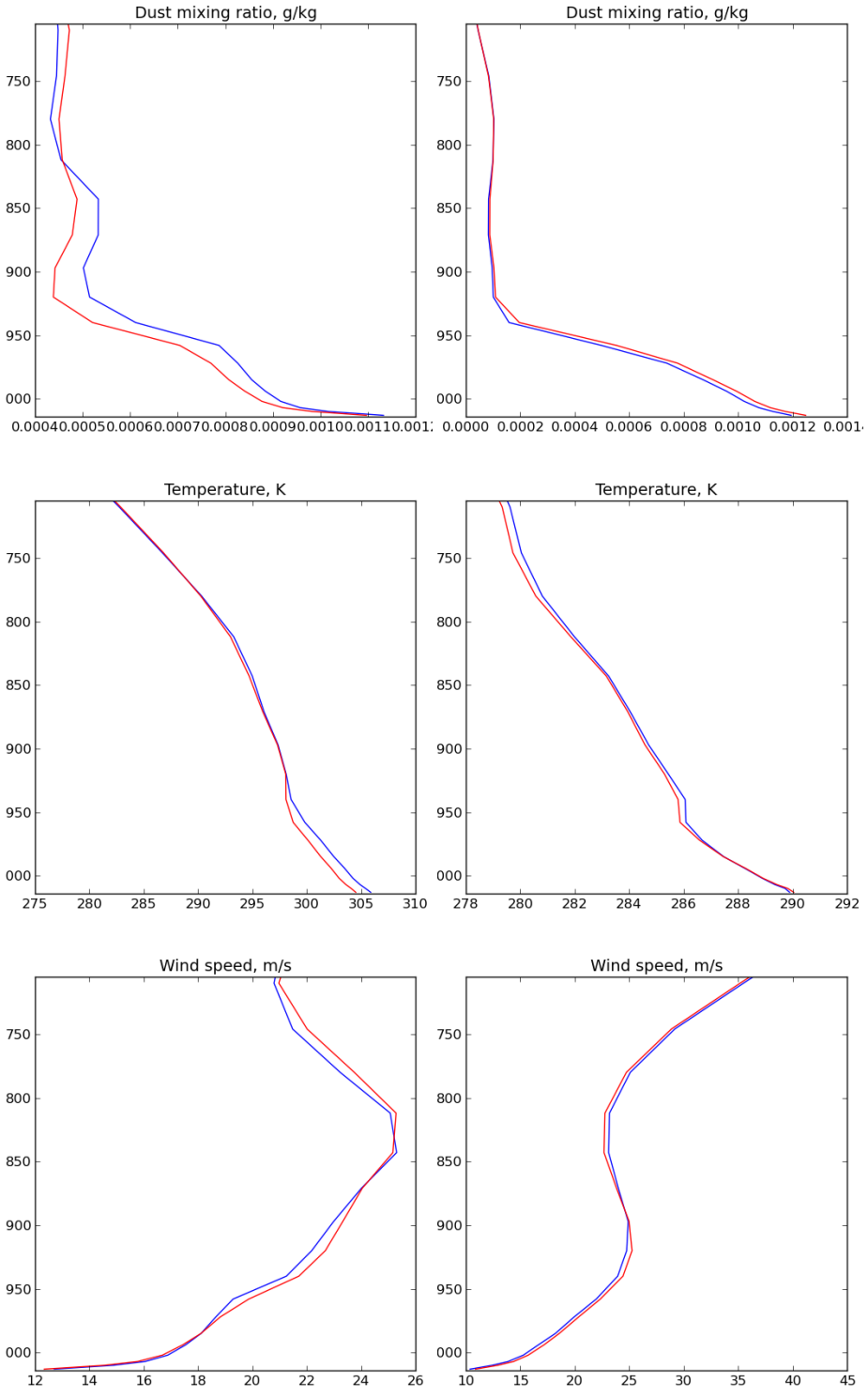

Fig. 16. Vertical profile of dust mixing ratio (top), temperature (middle) and wind speed (bottom) at Siwa Oasis. Forecasts starting on 17 April 2012 0UTC, lead time 15h (left) and 27h (right). REF is in blue, TOTAL in red.

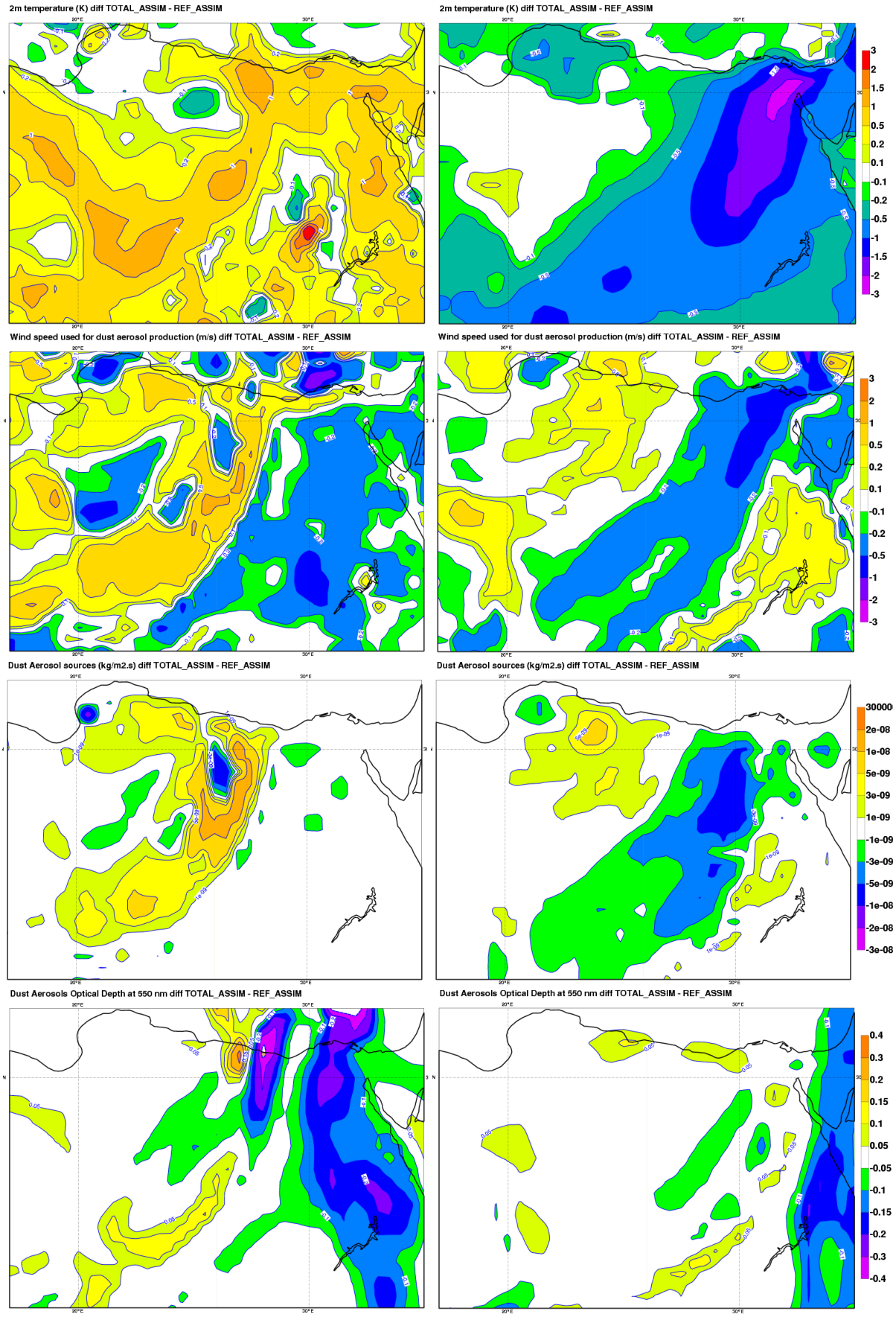

Fig. 17. Simulations starting on 17 April 2012, 24h forecast (left) and 36h (right) forecast time. Difference of TOTAL_ASSIM - REF_ASSIM for 2m temperature (top), 10m wind speed (middle top), dust production (middle bottom), dust AOD (bottom).

Table 1. Summary of the experiments carried out.

	Station		
Name	Short description	SW Dust-radiation computed with	LW dust-radiation computed with
NOAER	No dust	no dust	no dust
REF	Reference experiment	Tegen aerosol climatology	Tegen climatology
SW	SW dust-radiation interaction only	interactive dust	Tegen climatology
LW	LW dust-radiation interaction only	Tegen climatology	interactive dust
TOTAL	dust-radiation interaction	interactive dust	interactive dust
REF_ASSIM	reference experiment, initial conditions from assimilation	Tegen climatology	Tegen climatology
TOTAL_ASSIM	dust-radiation interaction, initial conditions from assimilation	interactive dust	interactive dust

Table 2. 2m temperature, RMSE of REF_ASSIM (left) and TOTAL_ASSIM (right) for forecast times 0, 12, 24 and 36h, average for the period of 10th to 25th of April 2012. Stations considered are Hurguada, Luxor, Kosseir, Siwa, Wadi el Natroon, Cairo, Port Said and Ras Sedr in Egypt, and Ben Gurion airport close to Tel Aviv in Israel.

Forecast time	0h	12h	24h	36h	48h
REF_ASSIM	1.46	1.48	1.5	1.62	1.53
TOTAL_ASSIM	1.32	1.49	1.43	1.6	1.58

Table 3. 2m temperature, bias of REF_ASSIM (left) and TOTAL_ASSIM (right) for forecast times 0, 12, 24 and 36h, average for the period of 10th to 25th of April 2012 over the same selection of weather stations as table 2.

Forecast time	0h	12h	24h	36h	48h
REF_ASSIM	-0.87	-0.05	-0.73	0.48	-0.47
TOTAL_ASSIM	-0.65	-0.18	-0.58	0.2	0.26

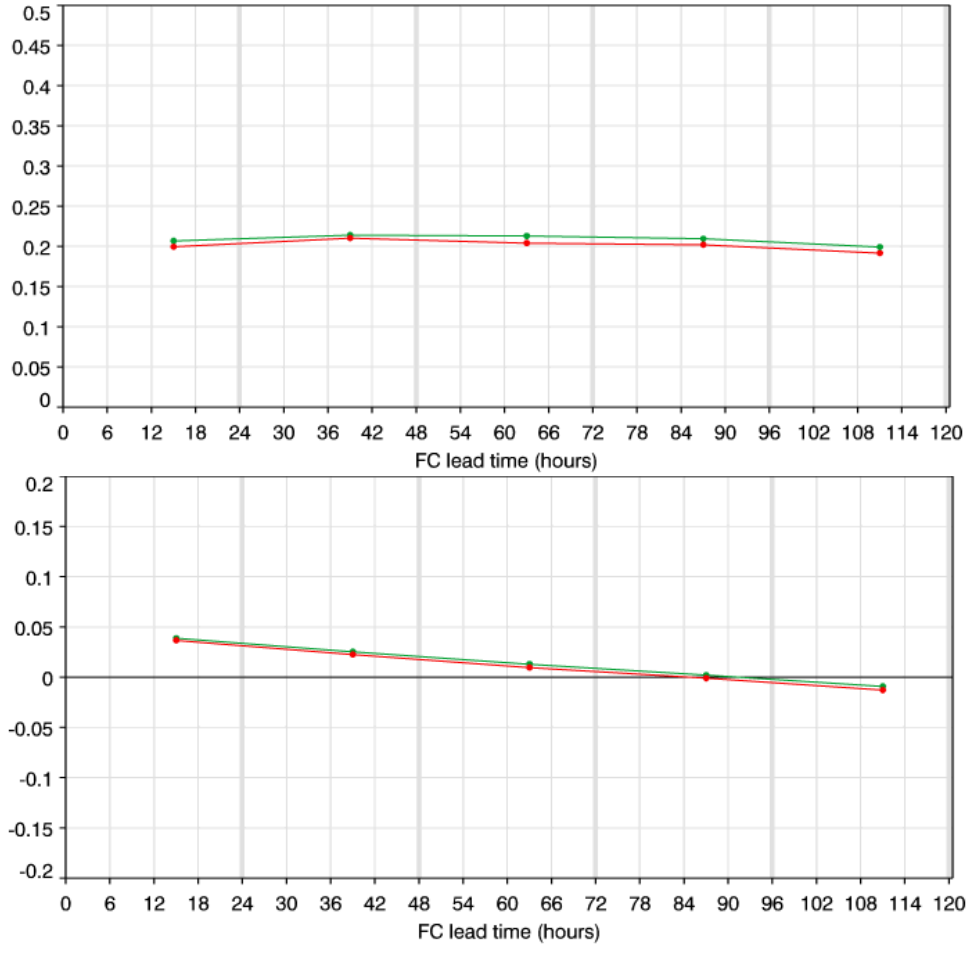

Fig. 18. RMSE (top) and bias (bottom) of forecasted total AOD against L2.0 Aeronet AOT at 500nm over 228 Voronoi-weighted sites globally, as a function of forecast time. REF_ASSIM is in green, TOTAL_ASSIM in red.